UNIL | Université de Lausanne
Faculté des géosciences
et de l'environnement

Master of Science in Geography

A framework for using Unmanned Aerial Vehicles (UAVs) and SfM photogrammetry to detect salmonid redds

Matteo Roncoroni

Under the direction of Prof. Stuart Lane
Expert : Prof. Grégoire Mariéthoz

Maîtrise universitaire ès sciences en géographie | Août - 2018

Acknowledgements

In these months I have shared with many people discussions about my research and funny moments on the field. In particular, I would like to thank:

My family and in particular my Mother

Prof. Stuart Lane, my thesis director, for his help, for his availability during my project and for allowing me to undertake this research

PhD student Gilles Antoniazza for his help and availability during my project

My friends and those with whom I shared great moments in the field throughout these years here in Lausanne.

Kurt de Swaaf for his inspiring articles about my research on NZZ and Der Standard

Dr. Jakob Brodersen and PhD student Philip Dermond for sharing with me their interest in this research

Dr. Sébastien Nusslé for sharing with me his interest in this research

Eva Baier for sharing with me her interest in this research and for her feedback

The technical department of Vacallo and Mirco Ricci (from the national Border Guard) for giving me permission to fly the drone on the Breggia river

And all those lent me a hand during my project.

Thank you

Summary

Salmonid populations are widely spread around the world and they are of both economic and ecological importance. The preservation and restoration of salmonid populations is therefore fundamental. However, salmonid populations are stressed and threatened and so in decline in many parts of the world. Spawning habitat degradation is one of the causes of this decline.
Knowledge of spawning sites and the associated evolution through time is therefore fundamental to protect salmonid populations. At present, spawning areas are investigated and counted using visual records. However, this method has some weakness and it does not allow for a correct appreciation of the real extent of salmonid reproduction.
In this regard, this research develops a framework for using Unmanned Aerial Vehicles (UAVs) and SfM photogrammetry to detect salmonid redds through analysis of inter-epoch Digital Elevation Models (DEMs of Difference).
Our results suggest that the combination of UAVs and SfM photogrammetry and the consequent production of DEMs of Difference may detect more redds than the present method, allowing for a better and more precise detection of the spawning grounds.
Furthermore, we demonstrate that SfM-derived outputs might be used to extract useful information about spawning, such as redd density or female lengths, without disturbance of the spawning sites.

Key words: UAVs; Structure-from-Motion (SfM); Digital Elevation Model (DEM); DEMs of Difference (DoD); Salmonid spawning; Redds

Résumé

Les populations de salmonidés sont largement répandues dans le monde et revêtent une importance à la fois économique et écologique. La préservation et la restauration des populations de salmonidés sont donc fondamentales. Cependant, les populations de salmonidés sont stressées et menacées et donc en déclin dans de nombreuses régions du monde. La dégradation de l'habitat reproductif est l'une des causes de ce déclin.
La connaissance des sites de frayage et de leur évolution dans le temps est donc fondamentale pour protéger les populations de salmonidés. À l'heure actuelle, les zones de frayage sont étudiées et comptées à l'aide d'enregistrements visuels. Cependant, cette méthode présente certaines faiblesses et ne permet pas une appréciation correcte de l'étendue réelle de la reproduction des salmonidés.
À cet égard, cette recherche développe un cadre d'utilisation des véhicules aériens sans pilote (UAVs) et de la photogrammétrie SfM pour détecter les lits de frayage des salmonidés à travers la comparaison de modèles numériques de terrain (MNT de différence).
Nos résultats suggèrent que la combinaison des UAVs et de la photogrammétrie SfM et la production consécutive de MNT de différence peuvent détecter plus de lits de frayage que la méthode actuelle, permettant une détection et plus précise des frayères.
En outre, nous avons démontré que les résultats dérivés de la photogrammétrie SfM pourraient être utilisés pour extraire des informations utiles sur le frayage, telles que la densité des lits ou la longueur des femelles, sans perturber les sites de frayage.

Mots-clés: UAVs; Structure-from-Motion (SfM); Modèle Numérique du Terrain (MNT); MNT de différence (DoD); Reproduction des salmonidés; Lits de frayage

1. Introduction

Salmonid populations are widely spread around the world (Elliot, 1994; Crisp, 2000) and they are of both economic importance (e.g. Crisp, 2000), in particular the genus *Salmo* (e.g. brown trout or Atlantic salmon) and *Oncorhynchus* (e.g. rainbow trout or Pacific salmons), and ecological importance. For example, the lifecycles of Pacific salmons are strongly bound to Pacific Northwest forest ecosystems and terrestrial fauna such as food (e.g. bears, wolfs, eagles, etc.) (e.g. Quinn, 2005). The preservation and restoration of salmonid populations is therefore fundamental.

Borsuk et al. (2006) and Zimmerli et al. (2007) have described how brown trout populations are at risk in Switzerland, a risk that may extend throughout the Alpine arc, from France to Slovenia. Similarly, Hendry et al. (2003) have recorded serious degradation of salmonid populations in the British Isles. The Pacific Northwest territories are also suffering an important decline of salmonids, in particular Pacific salmons (e.g. Bradford and Irvine, 2000; Simenstad and Cordell, 2000; Quinn, 2005; Bisson et al. 2009). These authors argue that decline is related to different causes including climate change, over-fishing, water quality and habitat degradation. The latter is identified by Nehlsen et al. (1991) as the most important issue related to the diminution of salmons in the Pacific Northwest.

Degradation is thought to be a consequence of a wide range of possible factors, commonly associated with humans (e.g. construction of dams, land use, urban growth, etc.) and these factors may impact upon one or many stages of the salmonid life cycle, including spawning. Kondolf et al. (2008) argued that the decline of salmonid populations in the northern hemisphere can be attributed primarily to the degradation of spawning gravels, which obviously reflects a degradation of the spawning habitat itself. This makes quantifying the presence of spawning habitats, and their change through time, critical to understanding their natural dynamics but also to identify reasons for their long-term decline.

Thanks to improvements in hydrological and biological sciences, the spawning behavior of salmonids, the relationships between spawning and hydraulic conditions and the conditions that limit or enhance reproduction are well known (e.g. Crisp and Carling, 1989; Elliot, 1994; Crisp, 2000; Armstrong et al., 2003). However, there remain few data on the presence and number of spawning sites and their changes through time and even though data on the number of redds is likely to be crucial for understanding population dynamics (e.g. Rieman and McIntyre, 1996).

The most common means of detecting and counting salmonid spawning sites remains walking along river banks during the spawning season and making visual observations (e.g. Crisp and Carling, 1989; Riedl and Peter, 2013). However, this approach has some weaknesses. First, it is influenced by the experience of researchers and their ability to detect the signatures of redd morphology and sedimentology in riverbeds. Second, even if redd detection is normally straightforward and does not require considerable expertise, due to their particular shape, redds may be masked soon after their construction by sediments and algae or simply flattened by river flow, making them difficult to observe. Third, significant time is required to detect spawning sites. On the one hand, there is the necessity to walk river banks for several hundreds of meters to identify spawning at a meaningful spatial scale, the river reach (and ultimately the river-basin). Normally, redds are not concentrated in one specific reach, obliging the observer to walk for a long time in order to see them. On the other hand, it is fundamental to return to the river several times during the spawning season, which may last for many weeks. While the potential duration of the spawning season is commonly known, it is impossible to know exactly when a fish will spawn in the river investigated. The need to return to a river reach is compounded by

the possibility that redds will be progressively harder to see with time after their construction, making them easier to see with an important number of surveys throughout the season instead of a singular survey. This is why new methods for redd survey are needed.

In this sense, developments in remote sensing technologies provide an opportunity (e.g. Lejot et al. 2007; Westoby et al., 2012; Micheletti et al., 2015a; Micheletti et al., 2015b). First attempts at salmon redd counting were recently made using unmanned aircraft systems (Groves et al., 2016). Groves et al. used unmanned aircraft systems to provide an alternative visualization of redds, allowing for manual image identification rather than walkover visual identification. In this paper we seek to go further by showing how it is possible to detect redds through automated image analysis. Recent research in fluvial remote sensing (e.g. Tamminga et al., 2015; Woodget et al., 2015; Dietrich, 2016; Marteau et al., 2016) has shown that the morphology of shallow-water streams can be quantified using a combination of Unmanned Aerial Vehicles (UAVs) and Structure-from-Motion (SfM) photogrammetry, the latter used to extract three-dimensional morphological detail (Digital Elevation Models or DEMs) on stream bed surfaces. By comparing DEMs through time (DEMs of difference), changes can be detected. As redds have a distinctive morphological signature, an ellipsoidal shape characterized by a depression upstream and an accumulation downstream (e.g. Crisp and Carling, 1989), DEMs of Difference (DoD) should be a means of quantifying the presence of redds. Thus, the principal aim of this research is to develop a framework for the use of UAVs in detecting salmonid redds using photogrammetrically-based processing of acquired images. A second and subsidiary aim is to show that such information can be used to enhance our knowledge of salmonid spawning. This information includes knowledge of redd densities, redd locations on the riverbed, female lengths, timing of spawning and egg burial depths, which is a crucial element for fish biology (Crisp and Carling, 1989). A key advantage here is that it may be possible to acquire data without entering the water and so avoiding redd disturbance (e.g. movement of fines, etc.). The focus of the work is *Salmo trutta*, or brown trout, redds for a case study site in southern Switzerland. The paper begins by detailing the information that our framework should be capable of providing in relation to salmonid redds. Then we present an overarching framework for this kind of approach, making reference to established research on how to produce precise, high resolution 3D data on streambed morphology and its change through time. We detail the methodology that we used to test this framework for brown trout redds. The results are presented for the case-study and discussed in the final sections of the paper.

2. Spawning of brown trout and the structure of salmonid redds

In order to understand the methodology proposed in this research, it is necessary to review briefly current understanding of brown trout spawning and the structure of salmonid redds. The former identifies when sampling is needed and the latter provides critical information on the target precision and resolution of acquired data, and hence the required design of the image surveys.

2.1 Timing, spawning and construction of the redd

Spawning of brown trout takes place each year, generally from autumn (October) to late winter (February) in the northern hemisphere (Armstrong et al., 2003). Swiss populations of brown trout tend to spawn from October to January (Riedl and Peter, 2013). Spawning time depends on altitude (Riedl and Peter, 2013) and mean water temperature (Heggberget et al., 1988; Webb and McLay, 1996; Klemetsen et al., 2003), and consequently trout spawning occurs earlier at high altitudes (Riedl and Peter, 2013). Reproduction involves two main stages: i) search for the ideal site and erosion of the streambed by a femate trout; and ii) deposition, fertilization and burial of eggs.

In the first stage, the female trout searches for a site where conditions for spawning are apparently present (e.g. Crisp and Carling, 1989; Crisp, 2000), and these conditions have been related to local water velocity, water depth and grain-size (e.g. Armstrong et al., 2003). Additional parameters shown to be important include the ease of disturbance of the substratum (e.g. Kondolf, 2000) and the presence of a local down- or up-welling of current (e.g. Burner, 1951; Healey, 1991). In order to check the conditions, the female erodes the streambed with her body, creating a depression called a pit, displacing the grains just downstream (e.g. Crisp and Carling, 1989; Crisp, 2000). In this way, the female trout can check local conditions and evaluate their suitability (e.g Crisp, 2000). While the female erodes the streambed, one (normally the dominant) or more males stay in the proximity of the female waiting to fertilize the eggs (e.g. Crisp and Carling, 1989; Elliot, 1994; Crisp, 2000). If the conditions remain suitable after the initial erosion, the female increases the erosion (e.g. Crisp and Carling, 1989) and the second stage begins.

At the beginning of the second stage, the female continues to erode the streambed more and more frequently while the dominant male drives away the *beta* males (e.g. Crisp and Carling, 1989; Crisp, 2000). At that point, the female lays the eggs while the male fertilizes them (e.g. Elliot, 1994; Crisp, 2000). The female then buries them with sediments created by erosion of the surrounding streambed (Crisp and Carling, 1989). This process may be repeated several times in the same spawning process, creating more pockets of eggs in the same redd (e.g. Crisp and Carling, 1989; Crisp, 2000). After the final deposition, the female continues to cut the streambed in order to complete the burying phase but with a low frequency, while the males move away (e.g. Crisp and Carling, 1989). The result is a salmonid redd created on the streambed.

2.2 Redd structure

As described in Section 2.1, the resulting structure of spawning is the redd. This particular structure is the result of the different stages of spawning and the continuous erosion of the streambed made by the female trout. As illustrated by Crisp and Carling (1989) a salmonid redd is recognizable by its ellipsoidal shape, with a depression upstream, called a pit, and an accumulation downstream, called a tail (see Figure 1). Clearly, the tail volume is related to the volume of the pit because the first one results from the displacement of the grains from the second one. The redd size is related to the size of the

female trout (Crisp and Carling, 1989) and the dimension increases with the increment of female length. As noted by Crisp (2000), the redd size is approximately 3.5 times longer than the female length. However, following Crisp and Carling (1989) it is possible to estimate redd length from female length (and *vice versa*) in a more rigorous approach using different parameters (Figure 2, see also Section 4.3). In the same way, it is possible to estimate other horizontal dimensions (e.g. pit and tail width). Differently, in the literature there is no evidence regarding the estimation of the vertical dimensions, such as pit depth and tail height. However, Grost et al. (1991) found that pit depths normally range between 0.07 to 0.34 m while tail heights vary between 0.03 and 0.25 m.

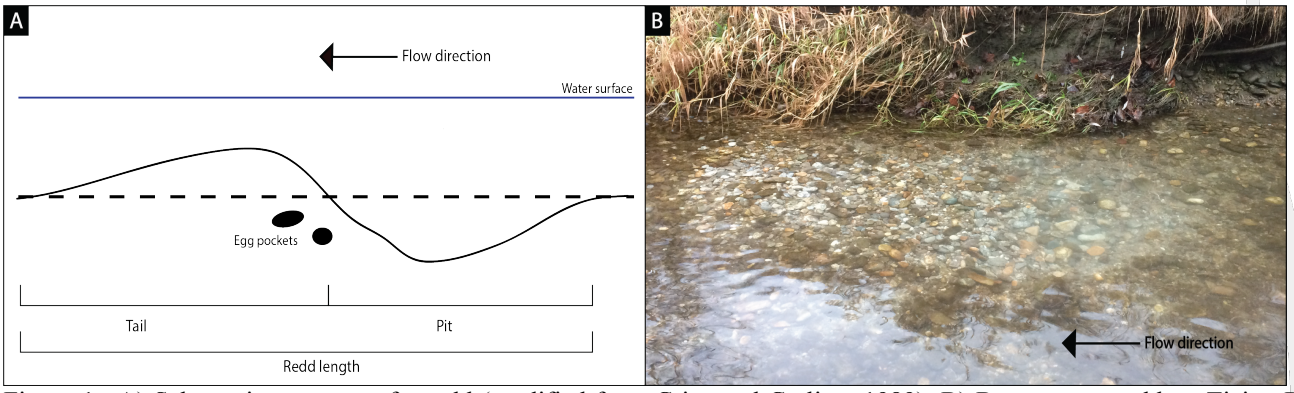

Figure 1 : A) Schematic structure of a redd (modified from Crisp and Carling, 1989); B) Brown trout redd on Ticino River (Switzerland)

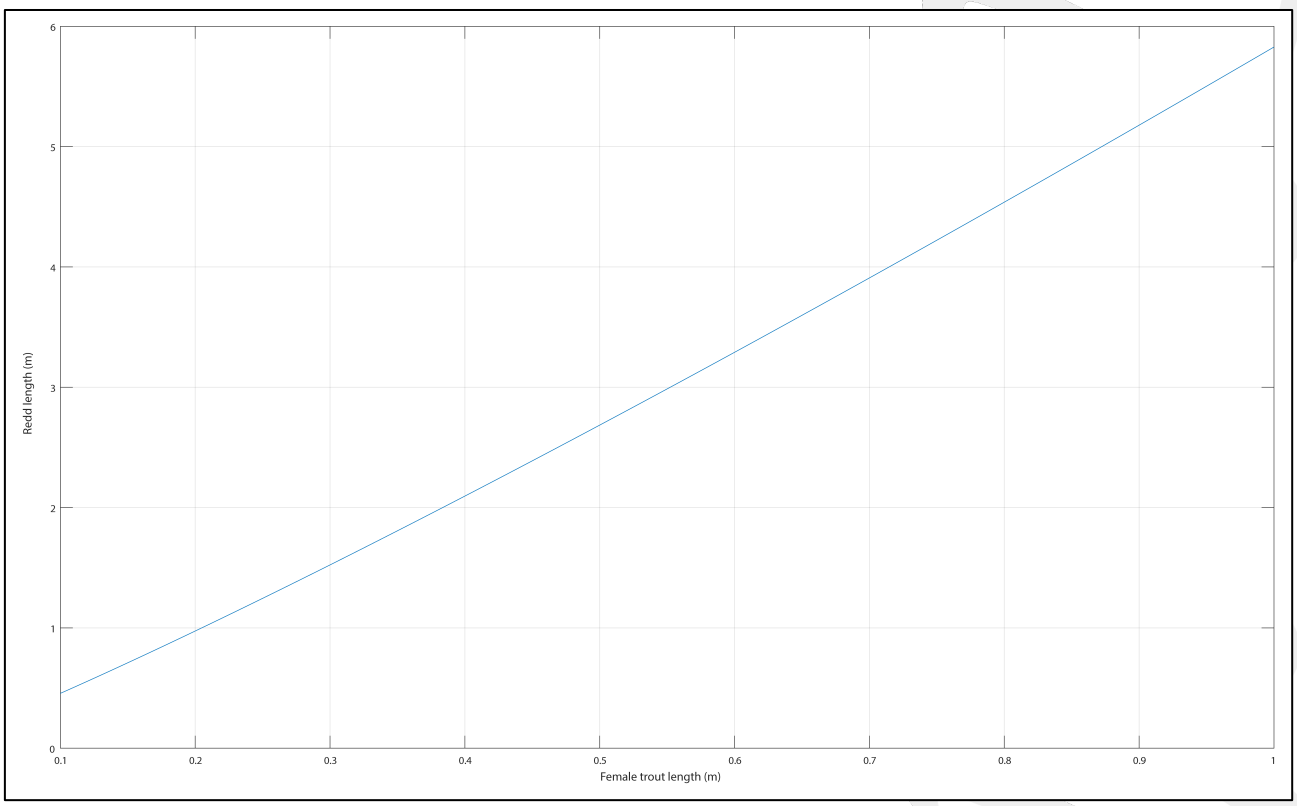

Figure 2: Relation between female length and redd length following Crisp and Carling (1989).

3. Development and justification of a framework for redd detection

Development of a framework for redd detection must consider the acquisition steps needed to allow a robust application of SfM photogrammetry, the methodology used to acquire DEMs from imagery in this application. It also needs to address how derived data are used to identify redds and to characterise their morphology. This section reviews the elements that were taken into account in the study test that follows in Section 4, making reference to what we know regarding the morphology of salmonid redds (Section 2.2).

3.1 Image acquisition platform

In order to switch from a visual system to a remotely-sensed system, imagery is necessary and this is likely to have to be near nadir because of refraction at the water surface. However, the rapid and easy detection of redds implies that the images acquired cover an important proportion of the river, from several to hundreds of meters at least. This requires an airborne image acquisition platform. Helicopters represent probably the most powerful vector to acquire photos and data of a river, allowing researchers to cover enormous distances faster than everyone else (e.g. Carbonneau et al., 2004, 2005; Bergeron and Carbonneau, 2012; Dietrich, 2016). However, this type of aerial vehicles is expensive and repeat deployment may not be affordable. The emergence of UAVs in science is providing an alternative, low-cost and flexible method to acquire images (Lejot et al., 2007; Carbonneau et al., 2012). The focus of this paper is the use of UAV-based imagery.

3.2 Extraction of elevation data

Recently, SfM photogrammetry has emerged in river research (e.g. Tamminga et al., 2015; Woodget et al., 2015), as an alternative to classical digital photogrammetry (e.g. Lane et al., 2000) due to a number of important advantages: it is rapid, automated, low-cost and easy to use by non-experts (Fonstad et al., 2013; Woodget et al., 2015). Moreover, and probably most importantly, if correctly applied it can produce high quality DEMs (e.g. Westoby et al., 2012; Fonstad et al., 2013), of a similar or better quality then those produced by airborne LiDAR (Fonstad et al., 2013).

As with classical digital photogrammetry, SfM produces 3D data from overlapping images (Westoby et al., 2012; Fonstad et al., 2013). However, unlike traditional aerial photogrammetry, where images overlap in parallel strips captured from parallel flights (Fonstad et al., 2013), SfM photogrammetry can use overlapping images captured from any given point of view (Westoby et al., 2012; Fonstad et al., 2013). As with terrestrial photogrammetry (Lane et al., 1994), oblique imagery can be used. Automated processing of oblique imagery was challenging using classical stereo-matching methods. SfM was conceived to address this by using machine vision methods such that oblique images can be analyzed automatically using even very low-grade quality sensors such as smartphones (e.g. Micheletti et al., 2015b). The basis of the machine vision approach is the Scale Invariant Feature Transform (SIFT) (Lowe, 1999), which allows identification of conjugate features in different images even if they have differences in viewpoint and resolution (e.g. Westoby et al., 2012; Fonstad et al., 2013). This is possible because these kinds of algorithms use brightness and color gradients to identify conjugate features and not, as with stereo-matching in classical photogrammetry, absolute pixels values (e.g. Fonstad et al., 2013). Unlike classical photogrammetry, SfM uses the collinearity equations, which describe the three-dimensional relationship between the sensor position and orientation and the ground surface, differently (e.g. Fonstad et al., 2013; Woodget et al., 2015). Whilst in traditional photogrammetry they are solved

after the introduction of GCPs, in SfM photogrammetry these equations can be solved before (e.g. Fonstad et al., 2013). SfM constructs a first and sparse 3D point cloud in an arbitrary coordinate system that, in a second phase and if it is needed, is transposed into a real-world coordinates system by the introduction of GCPs (Fonstad et al., 2013). Thus, SfM photogrammetry needs fewer GCPs unlike traditional photogrammetry, which requires a large number of GCPs (Westoby et al., 2012; Fonstad et al., 2013). More recent research has shown that GCPs may also be needed to improve camera calibration (James et al., 2017) and so introduced before production of the sparse 3D point cloud. After reconstruction of the sparse point cloud by the solution of collinearity equations, a point cloud can be generated with a resolution that is typically 3 to 5 times the image pixel resolution.

Two points merit additional discussion. First, the reason that image acquisition needs careful attention (see below) is that SfM photogrammetry can produce systematic errors (James and Robson, 2014; Carbonneau and Dietrich, 2017). These errors and deformations are produced because of the way that SfM builds 3D scenes (e.g. Fonstad et al. 2013), at the beginning from conjugate features identified by the SIFT process. With consumer-grade camera lenses (as typical of UAVs), this is a particular problem (Carbonneau and Dietrich, 2017) and means that the geometry of data acquisition, described below, is very important. Second, as noted by Fonstad et al. (2013), SfM is no different to classical photogrammetry that, whether manual or automated, requires good texture in the raw images so as to identify conjugate features. This is an issue for river survey because the presence of water, even if clear, may reduce image texture, so reducing the quality of the results obtained.

3.3 Theoretical precision and flying height

The design of image acquisition is based upon the target measurement precision for the elevation data needed to detect redds. The size of redds is likely to vary as a function of female lengths and species: for example, brown trout (*Salmo trutta*) redds are smaller than those of Chinook salmons (*Oncorhynchus tshawytscha*). Thus, the study design used reverse error propagation to identify the image acquisition necessary to detect the erosion and deposition associated with redd construction and spawning. Under the assumption that errors in Digital Elevation Model (DEM) are random, Gaussian and independent, a change in elevation between two dates has an uncertainty (U_{crit}) defined by:

$$U_{crit} = \pm t\sqrt{(\sigma_i)^2+(\sigma_j)^2} \quad [1]$$

where t is set for a given confidence interval, here taken as 95% (so t = 1.96) and σ_i and σ_j are the precisions of elevation of the two analysed DEMs (e.g. Brasington et al., 2000; Lane et al., 2003). In photogrammetry, it is well established that the theoretical precision of DEM elevations is approximately the same as the image resolution R (e.g. Lane et al., 2010). Under the assumption that the images are both acquired with the same study design:

$$U_{crit} = \pm 1.96\sqrt{2R^2} \quad [2]$$

Thus, the image resolution required to detect change is:

$$R = \left[0.5\left(\frac{U_{crit}}{1.96}\right)^2\right]^{0.5} \quad [3]$$

R can be defined approximately through:

$$\frac{p}{f} = \frac{R}{H} \quad [4]$$

where p is the sensor pixel resolution, f is the sensor focal length and H is the sensor flying height. Thus, we can determine the H needed in the first flight path to obtain a given U_{crit} as:

$$H < \frac{f}{p}\left[0.5\left(\frac{U_{crit}}{1.96}\right)^2\right]^{0.5} \quad [5]$$

3.4 Image acquisition geometry

Whilst [5] may determine the minimum flying height needed for change detection, this does not deal with the potential problem of systematic error in DEM surfaces which can arrive due to uncertainties in sensor position and orientation (e.g. Lane et al., 2004) as well as poorly reconstructed sensor geometry. The latter has been found to be a particular issue with UAVs as these tend to use low grade sensors with high levels of distortion and lead to artefacts in derived DEMs such as doming (Fonstad et al., 2013; James and Robson, 2014; Carbonneau and Dietrich, 2017). As shown by Wackrow and Chandler (2011), James and Robson (2014) and Carbonneau and Dietrich (2017), such errors may be reduced through careful design of flight paths, to include convergent and off nadir images, multiple flight altitudes and a high degree of image overlap. The basic principle here is to reproduce the kind of geometries long-used for calibration of non-metric cameras in photogrammetry (e.g. Robson, 1992). An example is shown in Figure 3, which combines at least two flying heights with some off-nadir imagery and two differently oriented flight paths (as not all geometrical distortions in the sensor are symmetrical). A minimum overlap of 70% is required for photogrammetric analysis but increasing the level of overlap to as high as 90% may improve calibration. Finally, the UAV flight velocity should not be so high that it introduces image blurring.

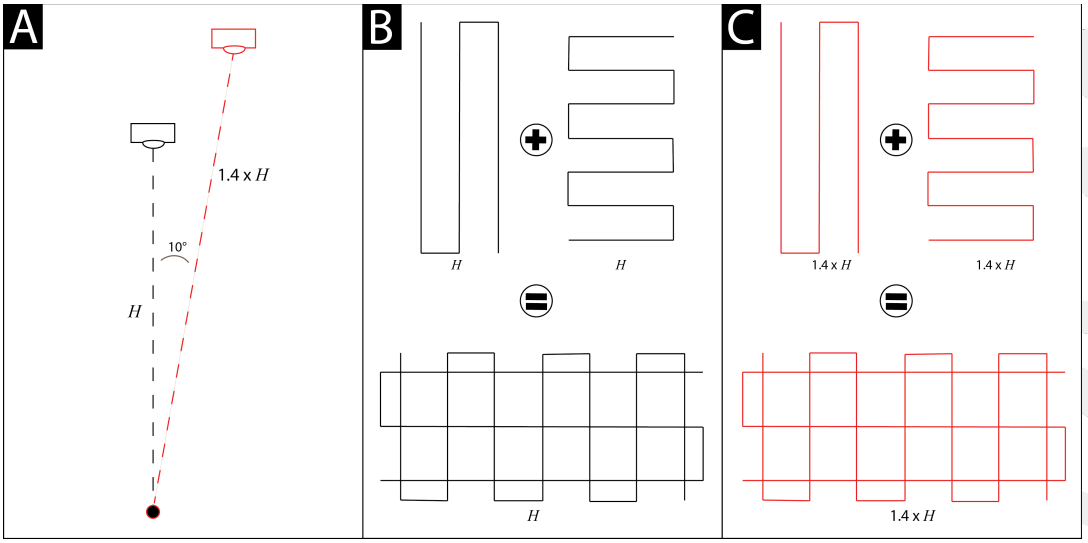

Figure 3: Flight paths strategy following Wackrow and Chandler (2011), James and Robson (2014) and Carbonneau and Dietrich (2017). A) Frontal view of two single acquisitions points where H = flight altitude of the 1st flight and 1.4 x H = flight altitude of the 2nd flight; B) Upper view of the flight path grid at H; C) Upper view of the flight path grid at 1.4 x H.

3.5 Ground control points

Early applications of SfM claimed that it may free the need for ground control points (GCPs) to be installed prior to image acquisition and that only a small number would then be needed for addition *a posteriori* if absolute orientation, position and scale was required (Fonstad et al., 2013). However, it has been shown that carefully located GCPs can reduce image deformation (James and Robson, 2014) and improve morphological change detection (e.g. Woodget et al., 2015). For orientation, position and scale, at least 3 GCPs are needed (e.g. Woodget et al., 2015) but more may help to avoid erroneous data transformations (Westoby et al., 2012) and ultimately to reduce systematic error (James et al., 2017) (Figure 4).

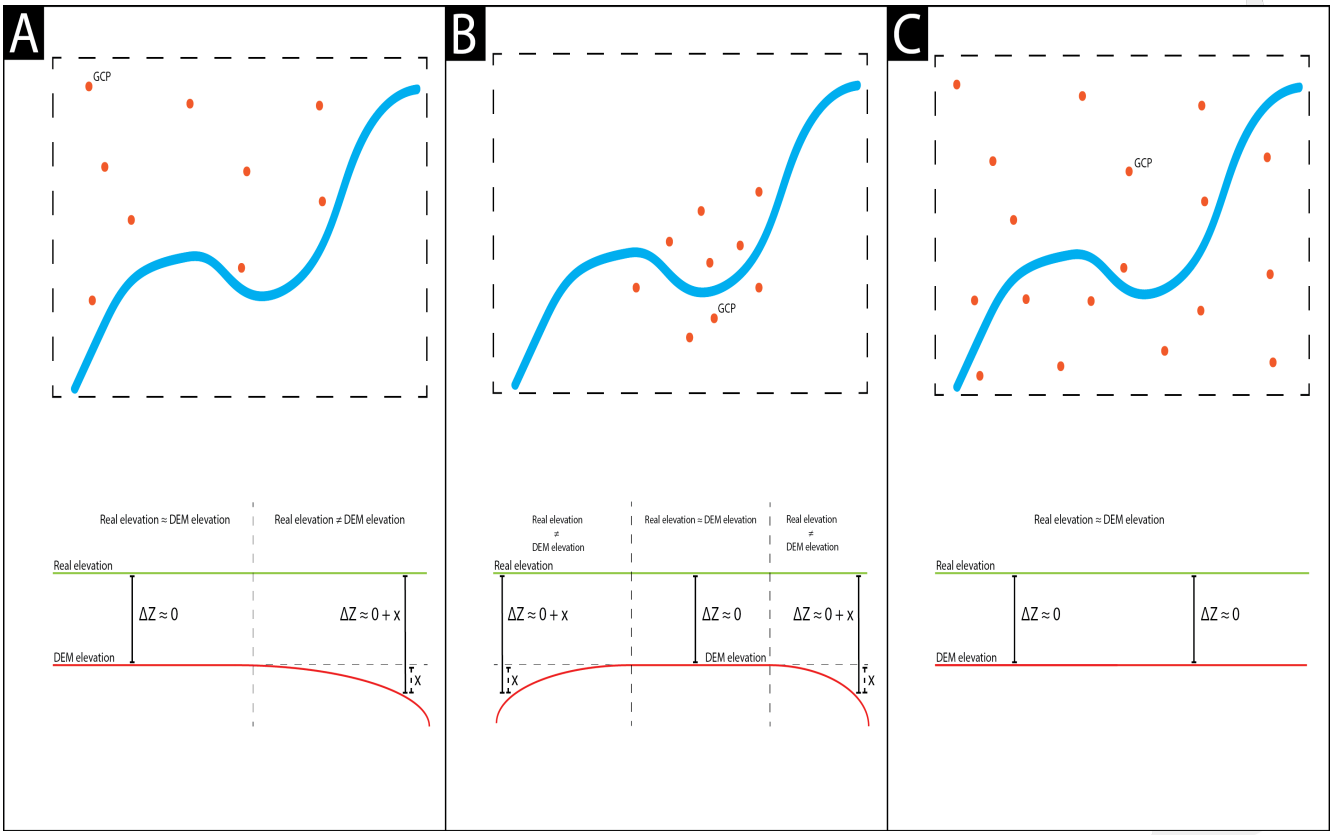

Figure 4: Systematic error may appear with a poor consideration of GCP locations. In 3A, GCPs are located only on one side of the river creating a non-regular tilt effect of **ΔZ**=0+x (where x is the difference between the real elevation and DEM elevation for the same spatial point) on the other side. In 3B, GCPs are located in the center of the study area creating a non-regular tilt effect of **ΔZ**=0+x on the both sides of the area (similar to doming effect). In 3C, GCPs are scattered across the study area better constraining the results and reducing the level of systematic error.

3.6 Post-processing: bathymetry correction

A crucial stage in automated redd detection using DEMs is the correct characterisation of stream bathymetry: as described by Fryer (1983), Fryer and Kniest (1985), Westaway et al. (2000, 2001), Butler et al. (2001) and Dietrich (2017), DEMs of submerged environments are affected by refraction at the air-water interface, which causes an underestimation of water depth and a consequently incorrect estimation of riverbed bathymetry. The magnitude of this effect changes as a function of flow depth, and hence discharge, and so if data is collected on two different dates, with different discharges, the effect has to be removed from both datasets for true changes to be detected. Tamminga et al. (2015) and Woodget et al. (2015) used a simple procedure to correct submerged areas of DEMs based on SfM

photogrammetry with near-nadir imagery. The principle follows Westaway et al. (2000): an uncorrected DEM is subtracted from his water surface elevations, the result is multiplied by the refractive index of clear water and then the new result is subtracted again from prior water surface elevations in order to produce a corrected DEM. Dietrich (2017) developed this approach to allow for off-nadir images, which violate the assumptions of simpler approaches (Dietrich, 2017). Dietrich's approach is based on the correction of each *wet-point* in the point cloud by solving the refraction equations for each camera that sees the *wet-point* itself and by then iterating the equations to convergence.

This per-camera and iterative approach is needed because each *wet-point* of the point cloud is seen from different flight altitudes and camera angulations. Considering this, a simple correction based on Snell's law or the simplified version of Snell's law as per Woodget et al. (2015) does not work on multi-view, multi-altitude and multi-directional imagery. Sources of errors in this correction approach still exist (Dietrich, 2017).

3.7 Redd detection: from visual detection to advanced morphological change detection

DEM analysis to detect redds represents a deviation from traditional visual detection (e.g. Crisp and Carling, 1989; Riedl and Peter, 2013) in that it is based upon determination of morphological changes rather than simply a visual analysis. The analysis requires two issues to be addressed. The first requires removal of any residual systematic error in the derived DEMs. Lane et al. (2004) showed that even with calibrated photogrammetric-grade sensors, random error in sensor position and orientation can lead to systematic error (e.g. tilt) in derived DEMs. Such tilt may be identified in validation data, or when two DEMs are compared and zones of no known change show apparent erosion or deposition. As such error is systematic, it can normally be modeled (e.g. using a two dimensional, non-linear fit to data that should show no change) and then removed. The second is addressed after removal of systematic error and involved quantifying the probable limits of detection (e.g. Brasington et al., 2000; Fuller et al., 2003; Lane et al., 2003; Wheaton et al., 2010; Milan et al., 2011), or minimum surface elevation changes, in the data. The simplest approach uses [1] but replaces the theoretical precisions with some measure of the actual elevation precisions achieved, under the assumption that the errors are Gaussian, random and pairwise independent (e.g. Lane et al., 2003; Fisher and Tate, 2006). Other approaches to identify when elevation differences are so small that they must be labeled as noise have been adopted. Such approaches recognize that error may not be spatially uniform and that applying this kind of detection limits may over-estimate the points labeled as error. For instance, Wheaton et al. (2010) showed that spatially extensive low magnitude changes, which in isolation may be too small to be detected using [1], may actually be real changes. This conclusion is reached because the changes are spatially coherent, and so the spatial organization of data within a DEM of difference should be taken into account.

3.8 Summary of key stages

The steps proposed in the previous sections are summarised in the dashed squares of Figure 5. Even if changes in parameters (e.g U_{crit}) must be addressed case-by-case, we recommend following the step-by-step methodology resumed in Figure 5. In this sense, changes in the workflow order might produce erroneous data. In particular, we refer to the post-processing phase (from bathymetry uncorrected DEMs to registered DEMs) that is crucial to obtain reliable data.

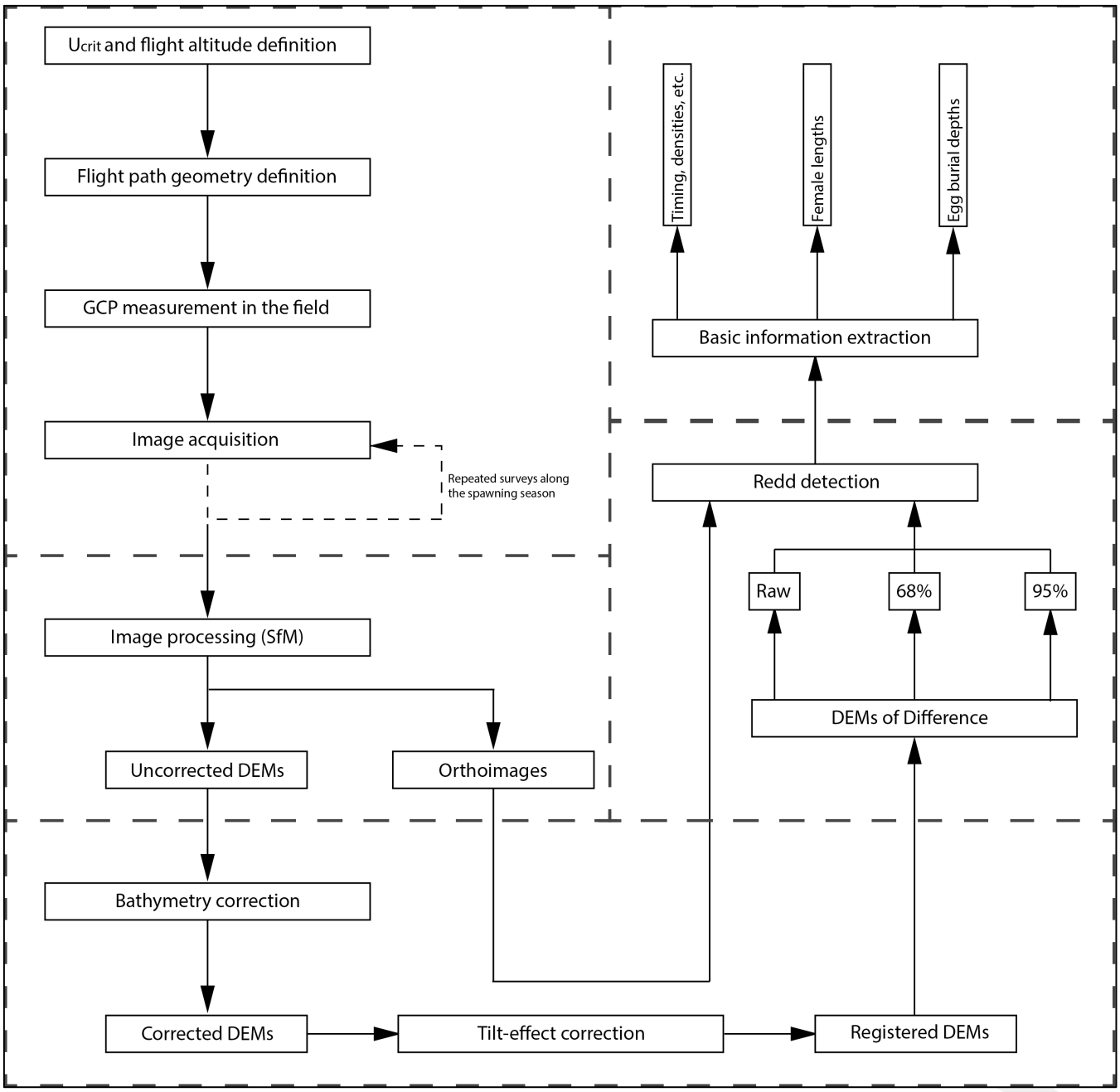

Figure 5: Methodological workflow. Each dashed square shows a different step of the proposed methodology to detect redds using the combination of UAVs and SfM photogrammetry.

4. Materials and methods

The aim of this section is to give an overview of the methods used to apply and to test the above framework for redd detection. Furthermore, we will show how we can extract useful information about spawning directly from the SfM-derived outputs (orthomosaics, DEMs and particularly DoD).

4.1 Case study

The Breggia is a Swiss river that runs in the southern part of Canton Ticino (Figure 6) from the appendix of Monte Generoso to Lake Como (Italy). The Swiss part of the Breggia has a catchment area of 81 km^2 approximately. The study site (Figure 6) is located northeast of Chiasso, in Pizzamiglio, in the lower part of Breggia, *c.* 3 km from Lake Como. Here, the Breggia flows through an urban area and its channel has been completely human-impacted (straightened with concrete banks). We chose this small reach (~70 m) mostly for two reasons: i) it is known to be a potentially important reach of the Breggia for spawning and ii) the small size compared with other upstream reaches allows us to focus upon testing the processing and post-processing phases. Upstream of this reach the river is concrete lined for 3 km, and no spawning is possible.

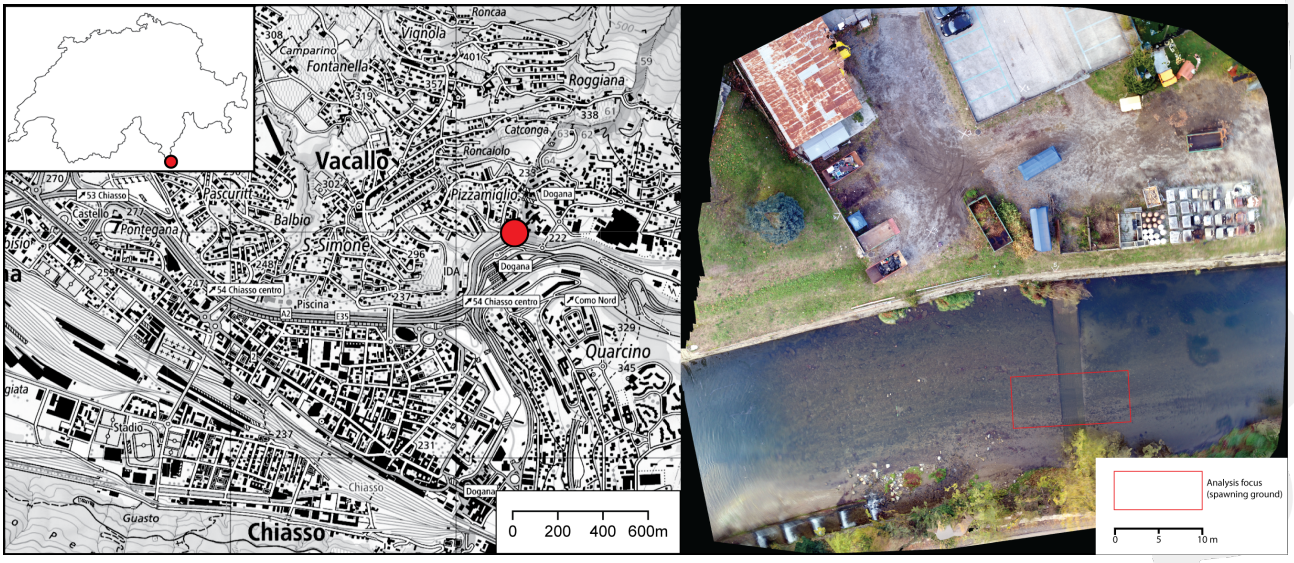

Figure 6: On the left, localization map of the studied zone (©swisstopo). On the right, orthomoisaic of the zone with boundaries of the focused area of interest. All of our further analysis (e.g. DoD) will be performed only on the focused area.

According to the literature (Riedl and Peter, 2013), we surveyed the reach 8 times during the spawning season between Oct. 7th and Dec. 30th 2017 (Oct. 7th, Oct. 20th, Oct. 28th, Nov. 11th, Nov. 19th, Dec. 2nd, Dec. 10th, Dec. 23rd and Dec. 30th), with a mean time interval between survey dates of 9.5 days. We focused the analysis on only three dates (Nov. 19th, Dec. 2nd and Dec. 10th): no redds were identified before Nov. 19th and, in the same way, no new redds were identified after Dec. 10th, although this was partly due to important sediment accumulation at our site between Dec. 10th and 23rd caused by in-stream works in the upper Breggia.

4.2 Redd detection through UAV-based SfM photogrammetry

4.2.1 Image and GCP acquisition

To acquire the raw images needed to create high resolution DEMs and orthomosaics we used the DJI Phantom 3Pro quadcopter. This drone is low cost, easy to use, lightweight, easy to transport and it has a built in GPS. Table 1 summarizes the drone's key characteristics. Crucially, software is available to aid flight planning which is necessary to make sure that imagery has the required resolution, coverage and geometry (see Section 3) aided by the built-in GPS.

Table 1: Phantom 3Pro specifications (further information available at http://www.dji.com/phantom-3-pro/info#specs).

Weight (battery and propellers included	1280 gr.
Max speed	16 ms^{-1}
Max flight time	Approx. 23 minutes
Global Positioning System	Yes
Camera	4K, 12.4 Megapixels
Operating software	Applications available for flight planning

Here, flight planning is undertaken with Pix4Dcapture, a freely availably flight planning application available for Android and iOS systems (Pix4D, 2017a). An U_{crit} of ±0.024 m was chosen and corresponds to a first flight altitude of ~20 m with a Phantom 3Pro. This U_{crit} reflects two main aspects: i) it is coherent with pit depths and tail heights recorded by Grost et al. (1991) and ii) Breggia site is used for spawning by resident and migratory brown trout. The first aspect suggests that our U_{crit} is lower than the normal vertical changes produced by spawning allowing for a precise detection. The second aspect reflects the fact resident trout, being smaller than the migratory (e.g. Jonsson and Jonsson, 1993), produces smaller redds, so requiring better precision to be detected.

Figure 7: Example of blurred and distorted raw image captured by the Phantom3Pro camera when the drone was changing direction. The camera tends to create this kind of artefacts with high flights velocities, reducing the quality of the photoset used in the 3D reconstruction.

A second flight altitude was set at 30 m (~1.4 times the first altitude) with the camera at 10° off nadir. Following the flight path geometries of Figure 3, we performed two flights at 20 m with two different path orientations (to obtain convergent images); the same was undertaken for the second flight

altitude. Second, to improve the quality of the final SfM outputs we also set an overlap of 90%. The flight speed was set to medium (according to the options of Pix4Dcapture) to avoid image blurring and distortion (Figure 7).

We painted GCPs on stable zones using a biodegradable white paint to make a large cross. We added a small red dot as a permanent marker. The white cross disappeared between surveys but the red dot remained so we could repaint the GCPs in subsequent visits. 5 GCPs were painted and measured with dGPS within the Swiss coordinate system.

4.2.2 Image processing

To create high resolution DEMs and orthomosaics from the raw images, we used the software Pix4Dmapper developed by Pix4D. Pix4Dmapper is able to produce fully geo-referenced high-resolution 2D orthomosaics and 3D elevation models with perspective distortions removed (Pix4D, 2017b). The workflow is divided into three main steps: i) initial processing; ii) point cloud and mesh generation and iii) DEM and orthomosaic production. In the first step Pix4Dmapper identified conjugate features across multiple images and used these to calibrate the external and internal camera parameters. An initial sparse point cloud was generated, which was used to insert GCPs and to geo-reference the cloud. As the raw images taken by our DJI Phantom 3Pro had WGS coordinates while our GCPs had Swiss CH1903+/LV95 coordinates, we converted the WGS coordinates to Swiss ones before the first processing step using the conversion system supplied by the Swiss Federal Office of Topography (SwissTopo®). In the second step, the sparse point cloud was densified to obtain a dense point cloud. In the third step a DEM was interpolated and an orthoimage free of perspective distortions was produced. An important by-product of all steps, but notably Step 1, is a quality report, which was used to assess the fidelity of the photogrammetric solution.

4.2.3 Bathymetric correction

Dietrich's (2017) bathymetric correction method was applied to deal with water refraction. First, the water surface was modeled from water edge data using kriging in a GIS framework. Second, the associated water surface was used to identify DEM elevations that were inundated. These were exported. Data on the relative positions and calibration of the camera were exported from Pix4D. Each point is then treated according to those images on which it appears and the associated collinearity equations to produce corrected elevations for inundated points. The only parameter that this analysis requires is the refractive index of water, which is here taken as 1.337 (Harvey et al., 1998). These were then recombined with the elevations from non-inundated zones in the GIS to produce a corrected DEM.

4.2.4 DEMs of Difference

DEMs of difference (DoDs) were calculated. Initial visualization of the results suggested that there was a systematic error, notably revealed by changes where there should have been none (e.g. in large boulders that would not have moved between the dates of acquisition). Here, we used the freeware CloudCompare, which can undertake the co-registration on two datasets using an iterative closest point (ICP) algorithm (see Besl and McKay, 1992). The principle of the ICP is to register a shape to her reference shape in order to minimize the distance, indeed the spatial error, between the two shapes themselves (Besl and McKay, 1992). In our case, two point clouds were registered each time. Following Besl and McKay (1992), ICP relates the uncorrected point cloud to the reference one (pairing step), then it calculates the spatial movements most able to reduce the mean square errors of the distances and

finally it displaces the uncorrected data points to fit to the reference. To do so, we assume that our two datasets were already approximately co-registered. As tilt could lead to erroneous bathymetric correction, we applied the tilt correction after the bathymetric correction.

The registration results were normally satisfactory with low RMSE between the reference DEM and the registered DEMs. We also found that the tilt had been removed.

In order to calculate the actual DEM precision and hence the level of detection, we identified zones of no known change and compared elevations, so as to calculate the standard deviations of error needed in [1]. We explored the effects of both a 95% level of detection (i.e. 1.96 in [1]) but also a 68% level of detection. To produce DoD we used our reference DEM (Nov. 11th), which was the closest in time to the first spawning event.

4.3 Data on redd characteristics

The basic information extraction – female lengths and egg burial depths – was undertaken using both DoD and orthomosaics to measure the tail of each redd, which was then used to derivate female length and then from the latter egg burial depth. This is possible thanks to prior studies (e.g. Ottaway et al., 1981; Crisp and Carling, 1989) that have shown correlations with tail length and female fish size, and with female fish size and egg burial depth. Following Crisp and Carling (1989), we can estimate female fish length from tail dimensions by:

$$\ln T = b \ln L + \ln a \qquad [6]$$

where L, the length of the female fish (cm), is defined by:

$$L = e^{\left(\frac{\ln a - \ln T}{-b}\right)} \qquad [7]$$

T is the redd tail length (cm), and ln a and b are constants (for the genus *Salmo*: $b = 1.2 \pm 0.2$ and $\ln a = 0.45 \pm 0.38$). From [7] it is possible to estimate the basal main egg pocket burial depth following Ottaway et al. (1981) as:

$$B_{depth} = c + d \ln L \qquad [8]$$

where B_{depth} is the basal main egg pocket burial depth, c and d are constants ($c = -37.7 \pm 12.1$ and $d = 14 \pm 3.3$). It is important to note that the semi-logarithmic relationship of Ottaway et al. (1981) was performed on the fork length of the female trout and not on the total length as in Crisp and Carling (1989) in [7]. However, we assume (mainly from photographs) that high differences between the fork length and the total length of brown trout do not exist (in the adult and mature life-stages). The use of Ottaway et al.'s (1981) semi-logarithmic relationship instead of Crisp and Carling's (1989) linear regression to estimate egg burial depth is pertinent because we can derive the main basal depth and not the mean depth. In this sense, we are more interested in the estimation of the basal depth to understand egg loss from washout or overcutting by later spawning trout, if we know the approximate lower location of the main egg pocket. However, as noted by Crisp and Carling (1989), predictions of egg burial depths derived by both equations are normally similar. That said, burial depth estimation remains uncertain (e.g. Crisp and Carling, 1989; DeVries, 1997).

Measurements of redd tails were easier on the DoD due to a clear distinction between the erosion and deposition zones. However, an estimation of redd tail sizes was also possible from orthoimagery, even if this was more difficult and less precise than that done on DoD. Even if tail lengths were similar between the two measurement ways, we opted for the more rigorous DoD approach.

To do so, we used as a starting point the first evidence of deposition (near the pit) and as end point the last depositional evidence, following the general angle of the redd itself.

We also realized in undertaking these analyses that redds were being constructed one on top of another and so it was also possible to look at the extent to which redd construction was leading to the washout of the eggs of previously constructed redds.

5. Results

The presentation of results is divided into three main parts. First, results derived from uncorrected DEMs – bathymetry and tilt uncorrected DEMs – are presented and compared with the corrected one. This part is needed to understand how crucial is the correction of raw data in order to detect accurately salmonid redds, instead of incorrect artefacts. Second, redd detection from orthomoisaics and DoDs is presented. Third, we present information about spawning we can extract from SfM-derived outputs.

5.1 Illustration of data post-processing steps

The aim of this section is to illustrate the steps described in Section 4.2.3 and 4.2.4, in order to show the importance of the post-processing phases.

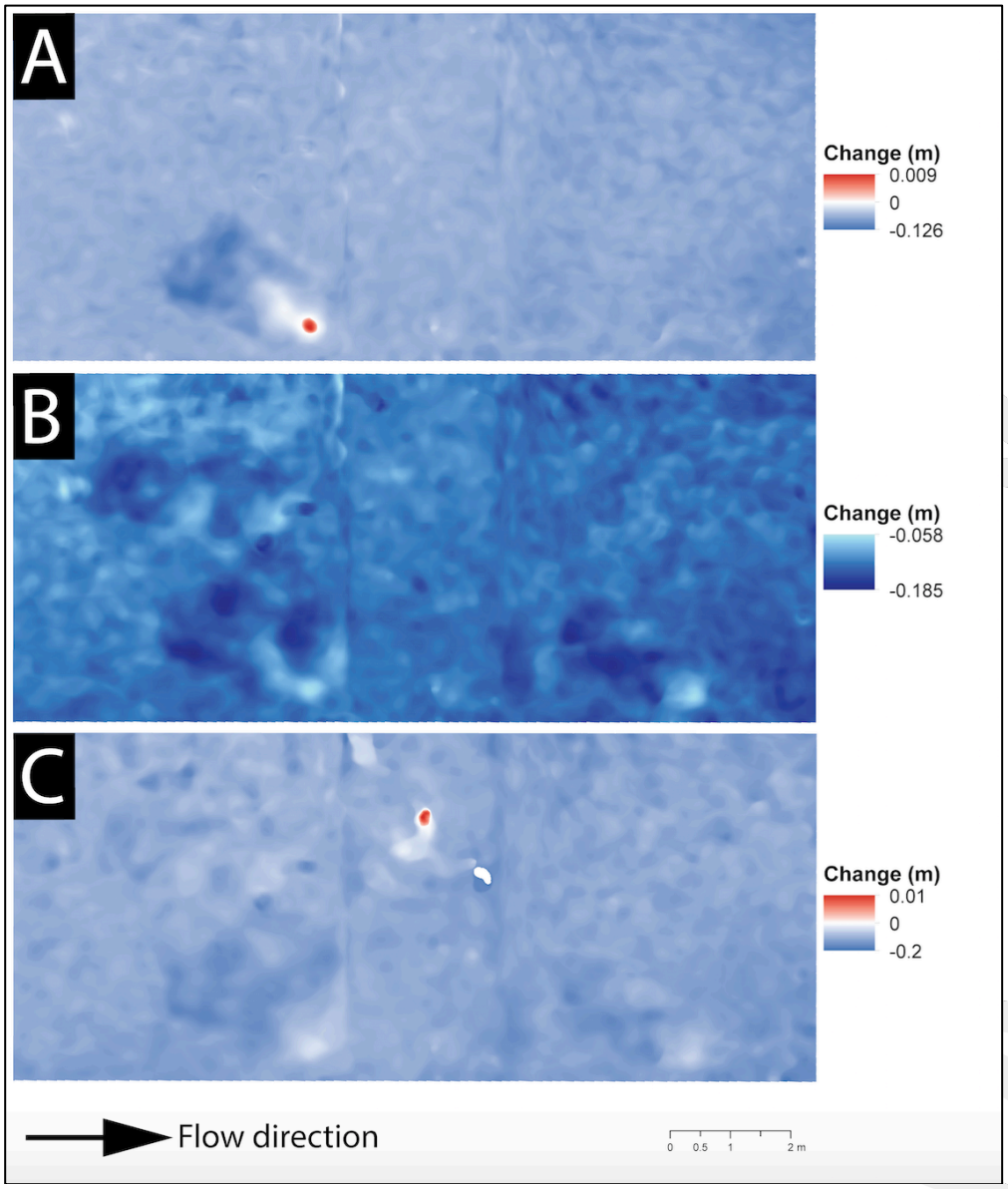

Figure 8: Raw DoD derived from original DEMs, therefore without bathymetry and tilt corrections. Sub-figure A shows the situation between Nov. 11th and Nov. 19th, sub-figure B between Nov. 11th and Dec. 2nd and sub-figure C between Nov. 11th and Dec. 10th.

Without prior correction of tilt and for underwater topography (Figure 8) the DoD is of no use for advanced change detection: erosion is dominant in the all three situations, and there appears to have been some more localised change that might suggest that spawning has occurred (e.g. in the bottom left of Figure 8A). Here, the tilt effect is strongly negative, which means that the Z-coordinates of our analysed DEMs are located at a lower spatial position than the reference (Nov. 11th).

The DEMs of difference after tilt correction in CloudCompare are shown in Figure 9. As compared with Figure 8, where the tilt strongly affects the quality of DoD, Figure 9 presents new DoD with lower tilt (in particular Figure 9B). Here, erosion is no longer dominant, and erosion and accumulation patterns are more balanced even if the latter is more present than the former (Figure 9A and C).

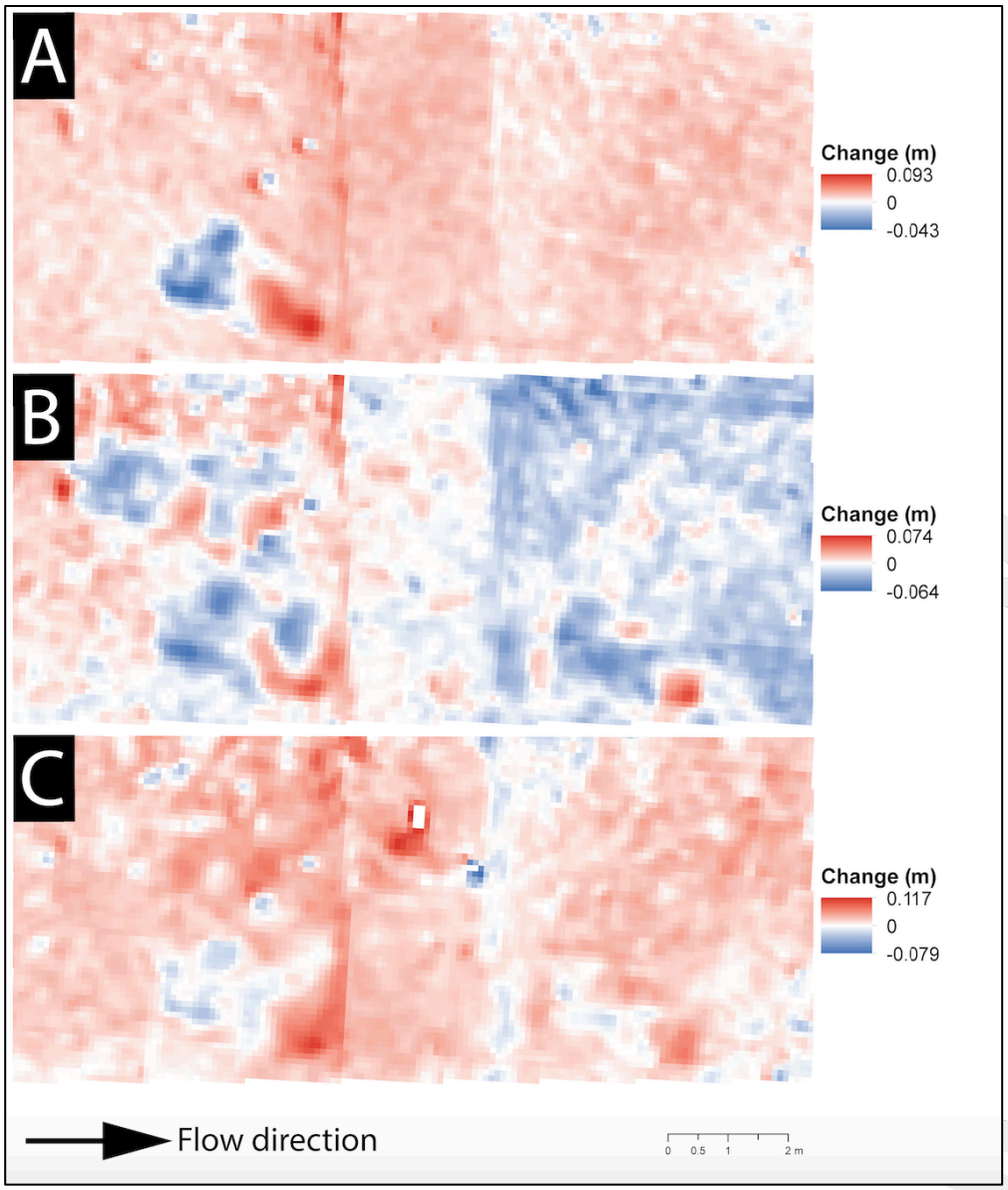

Figure 9: Raw DoD derived from DEMs with a first tilt effect mitigation. Sub-figure A shows the situation between Nov. 11th and Nov. 19th, sub-figure B between Nov. 11th and Dec. 2nd and sub-figure C between Nov. 11th and Dec. 10th.

Finally, with correction of both tilt and bathymetry (Figure 10) erosion and accumulation patterns become coherent. For comparison, Figure 11 shows the associated orthomosaics to allow for a visual comparison, in the sense that the zones of possible spawning shown in Figure 11 are also reflected in vertical changes in Figure 10.

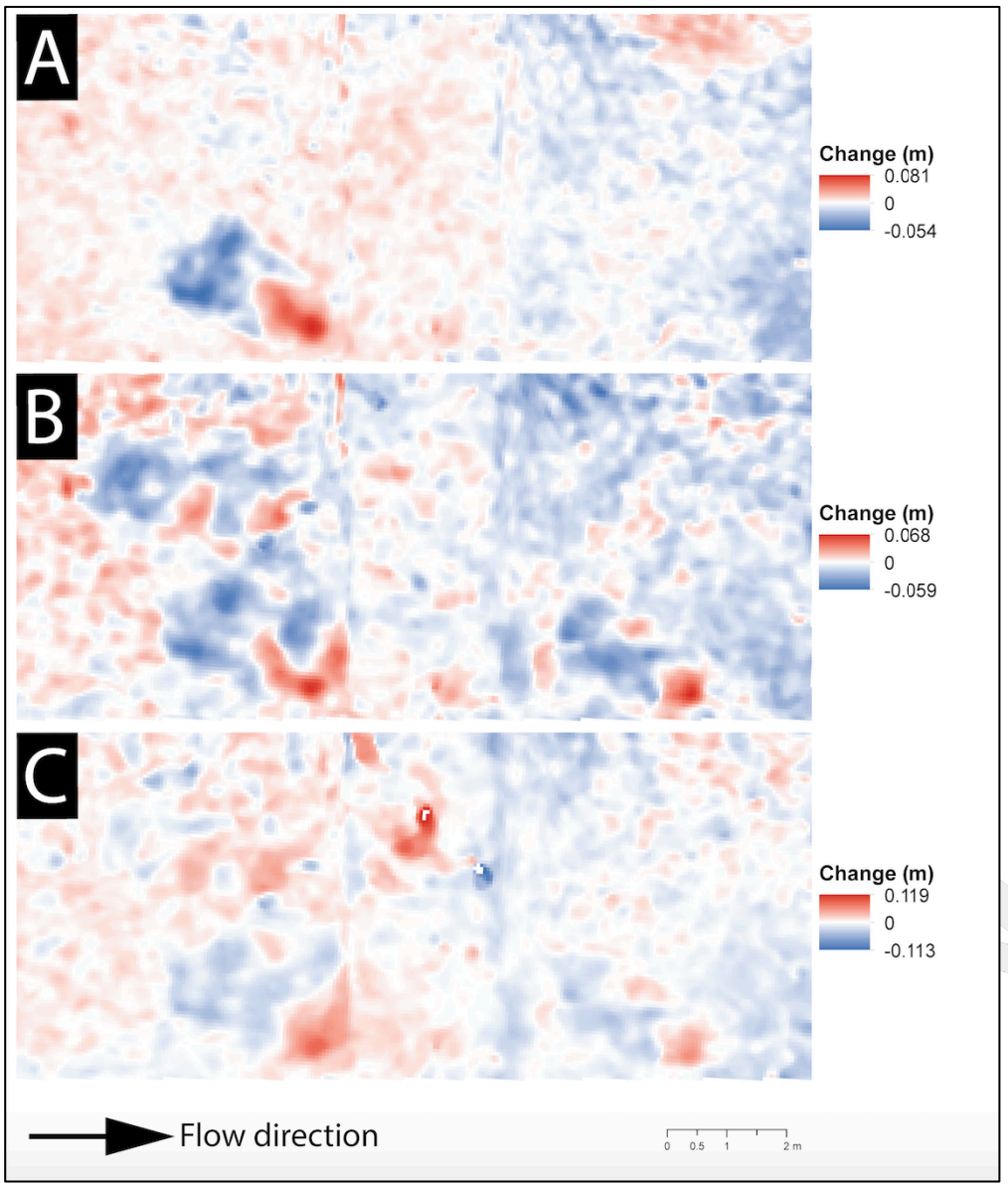

Figure 10: Raw DoD derived from bathymetry and tilt corrections DEMs. Sub-figure A shows the situation between Nov. 11th and Nov. 19th, sub-figure B between Nov. 11th and Dec. 2nd and sub-figure C between Nov. 11th and Dec. 10th.

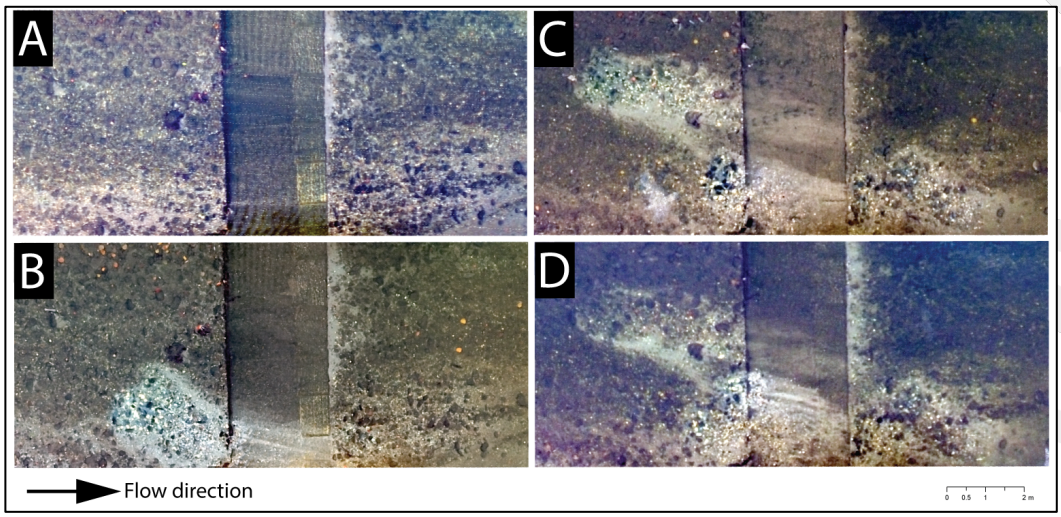

Figure 11: Orthomosaics of the spawning site. A) Nov. 11th; B) Nov. 19th; C) Dec. 2nd; D) Dec. 10th.

To assess the quality of the DoD results, Tables 2 through 4 show the mean and standard deviation of errors for zones of no possible change for the case of no treatment, tilt only and tilt combined with bathymetric correction. The distributions of error are shown in Figure 12.

Table 2: Mean errors and standard deviation of errors for the original DEMs calculated from the differences in elevations of fixed points (n=84) between the reference DEM (Nov. 11th) and the analysed DEMs.

	Nov. 11th - Nov. 19th	Nov. 11th - Dec. 2nd	Nov. 11th - Dec. 10th
Mean (m)	-0.070	-0.128	-0.124
Standard Deviation (m)	±0.009	±0.016	±0.013

Table 3: Mean errors and standard deviation of errors for the first tilt effect correction DEMs calculated from the differences in elevations of fixed points (n=84) between the reference DEM (Nov. 11th) and the analysed DEMs.

	Nov. 11th - Nov. 19th	Nov. 11th - Dec. 2nd	Nov. 11th - Dec. 10th
Mean (m)	0.016	-0.007	0.015
Standard Deviation (m)	±0.007	±0.018	±0.014

Table 4: Mean errors and standard deviation of errors for the bathymetry and tilt corrected DEMs calculated from the differences in elevations of fixed points (n=84) between the reference DEM (Nov. 11th) and the analysed DEMs.

	Nov. 11th - Nov. 19th	Nov. 11th - Dec. 2nd	Nov. 11th - Dec. 10th
Mean (m)	-0.001	-0.003	-0.006
Standard Deviation (m)	±0.010	±0.015	±0.013

As showed in Tables 2, 3 and 4, the mean errors between our reference DEM and our analysed DEMs decrease with each post-processing phase. In this sense, the mean errors of bathymetry and tilt corrected DEMs tend to 0 m, which indicated progressive removal of tilt. As expected, the standard deviations of error (i.e. the variability about the means) do not change much, if at all as tilt only impacts mean error. The distributions confirm (Figure 12A) that before any kind of correction, errors are primarily negative. The corresponding raw DoD also reveals this, falsely suggesting widespread erosion. Tilt correction does not eliminate systematic error fully and deviations still persist (Figure 12B). Finally, after both corrections, errors are well distributed around the origin (Figure 12C). Nov. 11th - Dec.2nd and Nov. 11th - Dec. 10th show small remaining negative deviation, but this is now very small and < 0.01 m.

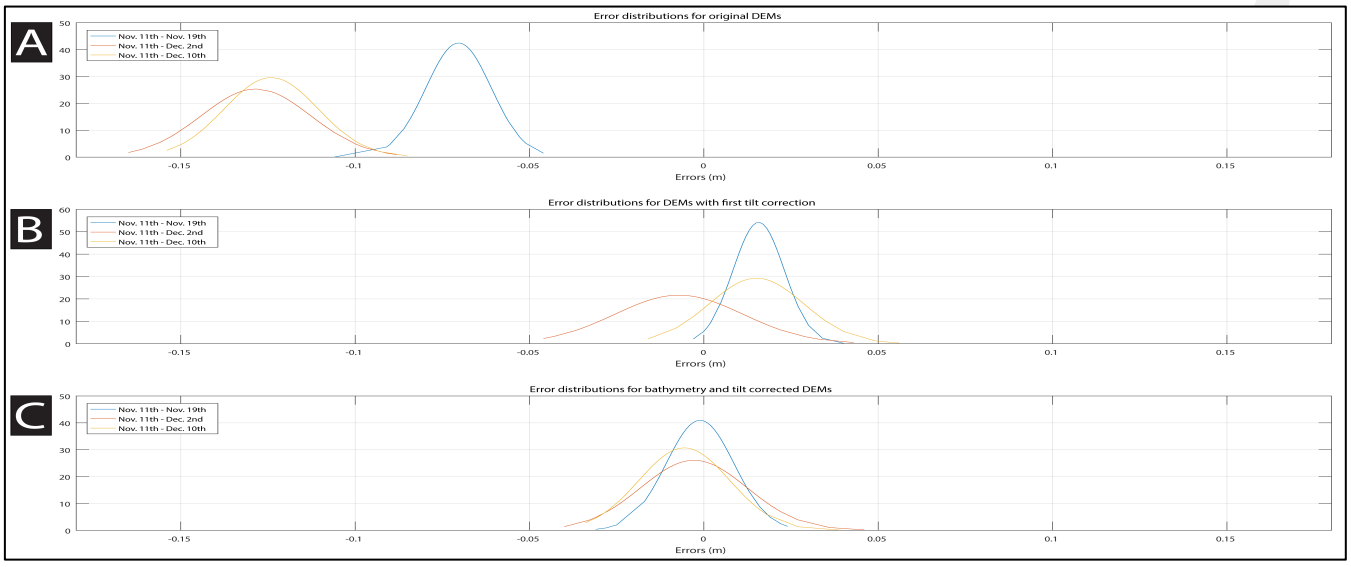

Figure 12: A) Error distributions for the original DEMs; B) For tilt corrected DEMs only; C) For bathymetry ant tilt corrected DEMs.

5.2 Redd detection

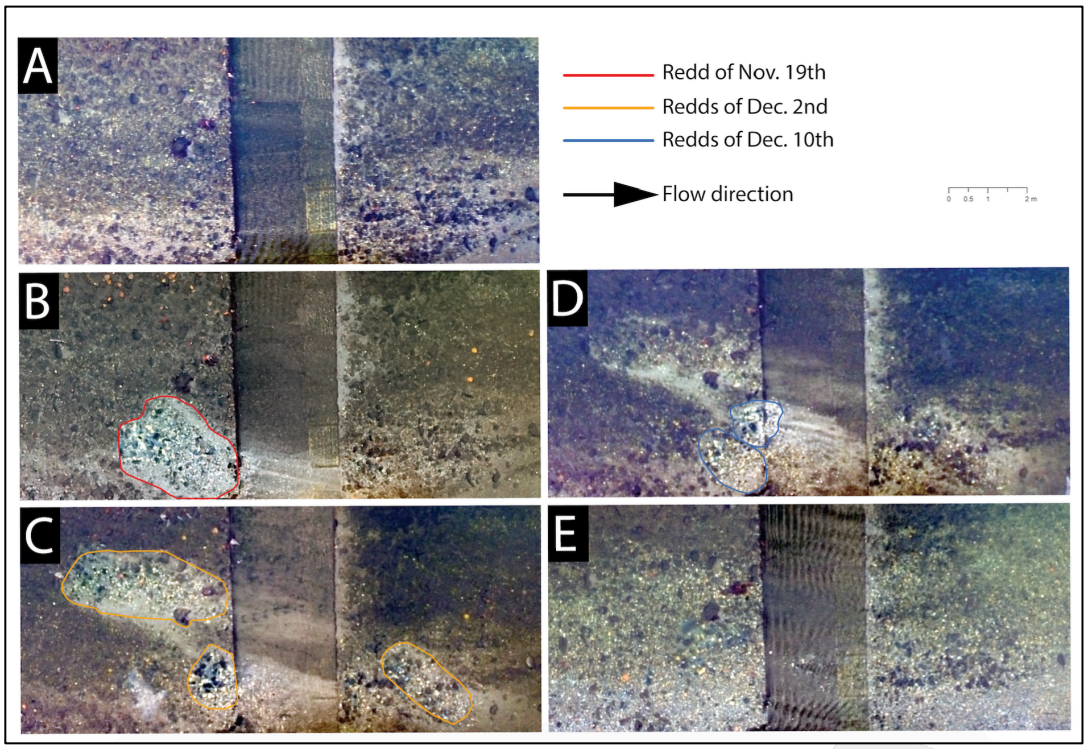

Figure 13: Evolution of the spawning site on the Breggia river throughout the 2018 season. A) Nov. 11th; B) Nov. 19th; C) Dec. 2nd; D) Dec. 10th; E) Dec. 23rd.

Figure 13 shows how redds disappear and new redds appear within the spawning season: the redd of Nov. 19th (Figure 13B) disappeared completely after 13 days (Dec. 2nd); the same happened to the redds that then formed by Dec. 2nd (Figure 13C) compared with Dec. 10th; and on Dec. 23rd (Figure 13E) no redds were still visible at the site.

Even before application of a level of detection threshold, Figures 14A and C confirm the presence of redds on the streambed, which were previously detected in Figure 13A and C. Figure 14B shows a different situation with 3 more supposed redds, and also some super-position. Once a 68% level of detection threshold is applied (Figure 15), the redds become clearer and this 10 m reach of stream has a total of 9 redds that form during the study period. These redds are much less clear when a 95% level of detection is applied (Figure 16) with only 8 of the 9 redds apparent in Figure 15 (see Table 5) and their morphology much less clear.

Table 5: Resumed results for the four different analyses performed on the Breggia spawning site.

Survey date	Nov. 19th	Dec. 2nd	Dec. 10th
Number of redds in the orthomosaics	1	3	2
Number of redds in the raw DoD	1	6	2
Number of redds in the 68% CL DoD	1	6	2
Number of redds in the 95% CL DoD	1	5	2

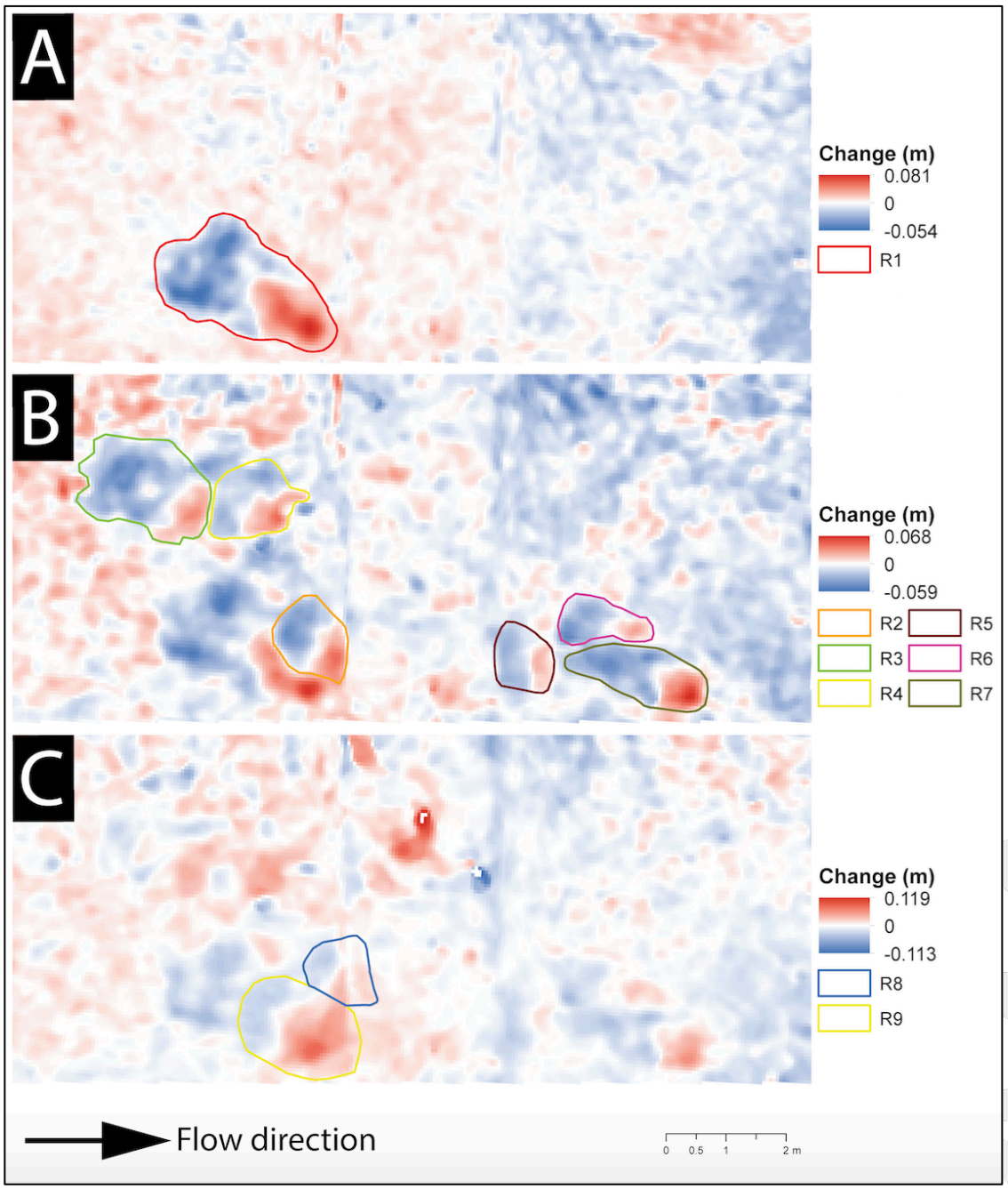

Figure 14: Morphological changes on the Breggia spawning site from raw DEMs. Sub-figure A shows the changes between Nov. 11th and Nov. 19th; sub-figure B shows the changes between Nov. 11th and Dec. 2nd while sub-figure C shows the changes between Nov. 11th and Dec. 10th.

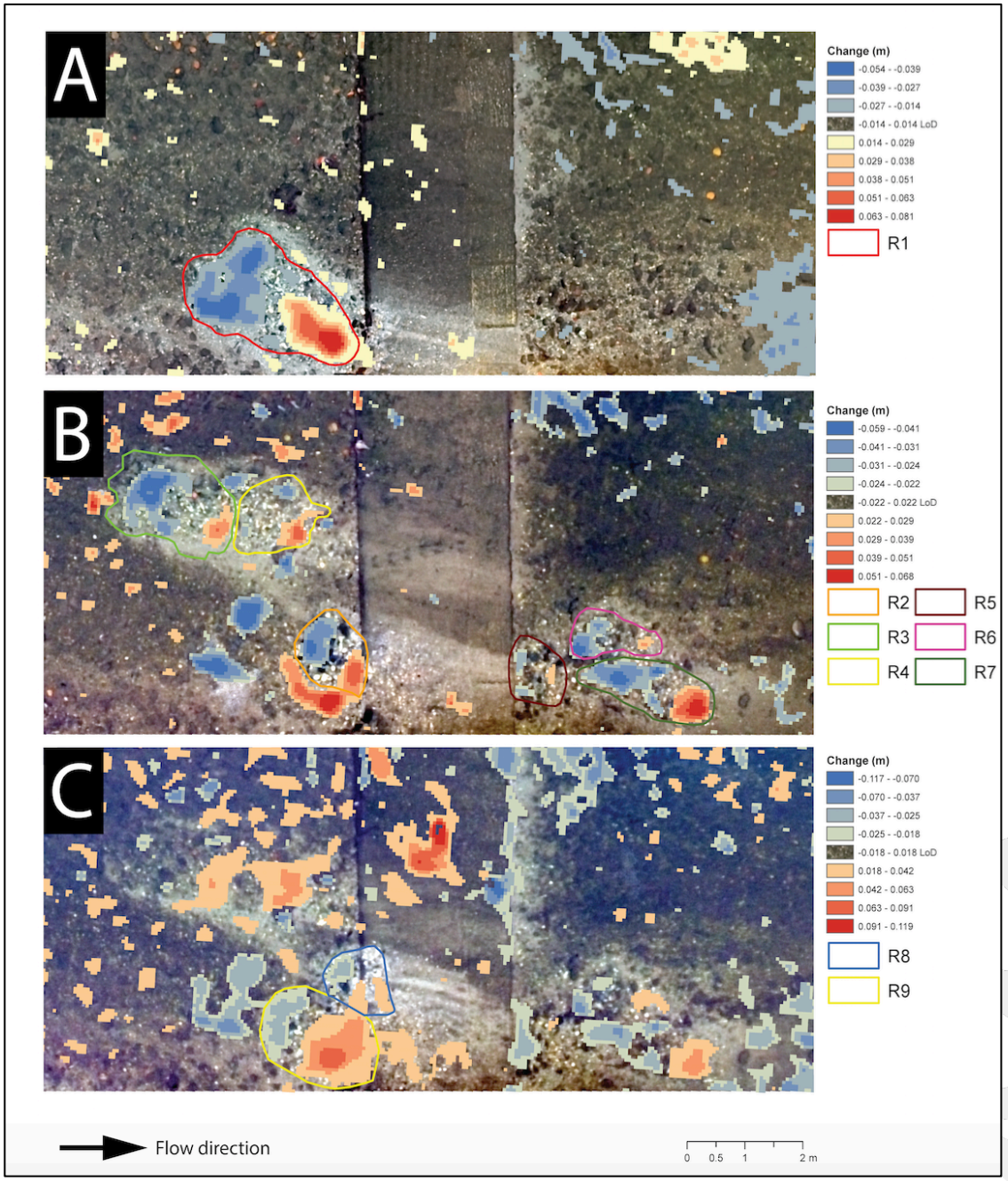

Figure 15: DEMs of Difference at the 68% confidence limit. Sub-figure A shows the changes between Nov. 11th and Nov. 19th; sub-figure B shows the changes between Nov. 11th and Dec. 2nd while sub-figure C shows the changes between Nov. 11th and Dec. 10th.

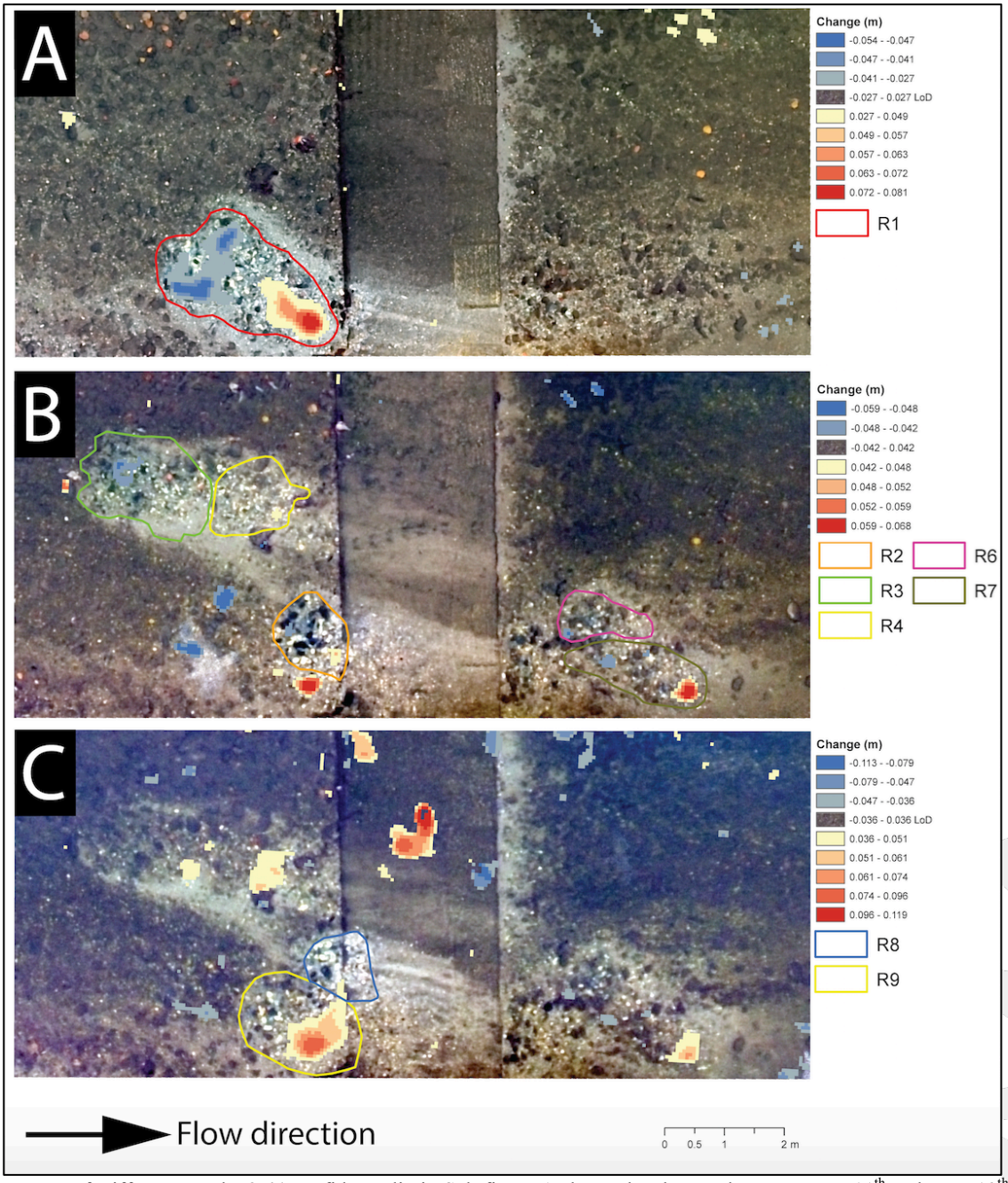

Figure 16: DEMs of Difference at the 95% confidence limit. Sub-figure A shows the changes between Nov. 11th and Nov. 19th; sub-figure B shows the changes between Nov. 11th and Dec. 2nd while sub-figure C shows the changes between Nov. 11th and Dec. 10th.

5.3 Data on redd characteristics

At the Breggia site, spawning began around Nov. 19th and it ended approximately around Dec. 10th, which means that the season was relatively short (21 days). The site used to spawn was small compared to the full area studied (Figure 17). In fact, trout used approximately ~77.8 m^2 out of ~849.4 m^2 (~9.2%) with a redd area of ~14.1 m^2 (based on redds identified using the 68% confidence interval).

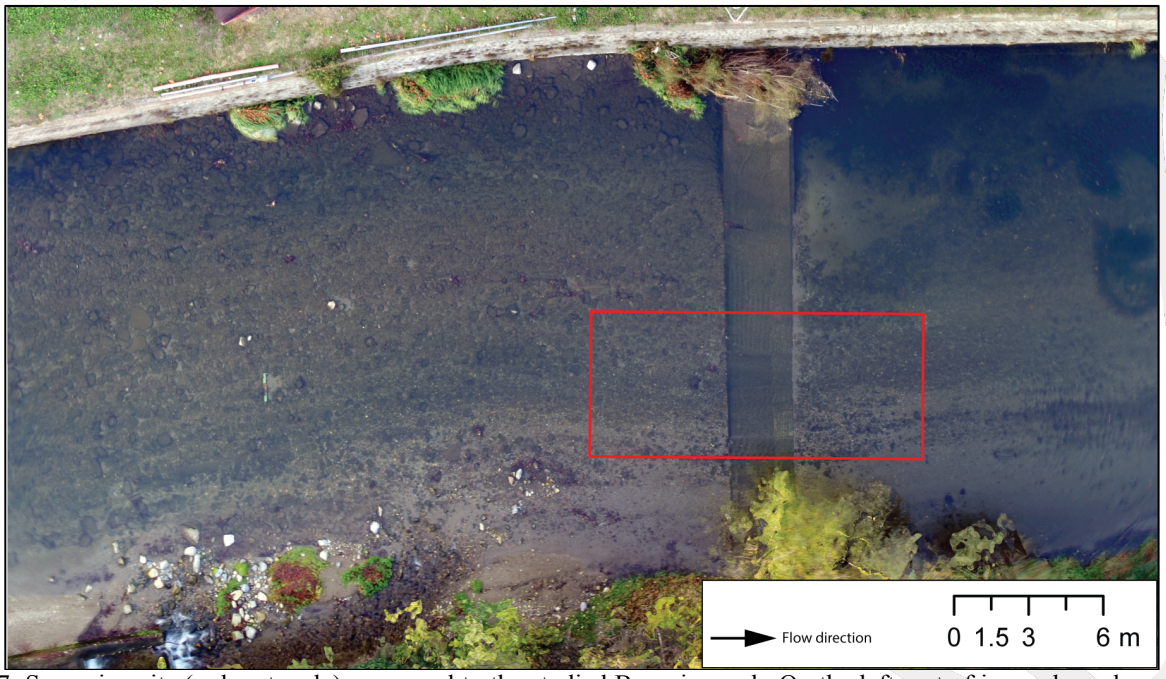

Figure 17: Spawning site (red rectangle) compared to the studied Breggia reach. On the left, out of image bounds, spawning habitat is limited by a deep pool generated by an artificial waterfall of ~4 m while on the right, out of image bounds, spawning is limited by a sandy and macrophytes-based pool. The orthomosaic presents the situation before spawning, on Nov. 11th.

Assuming that the 9 redds detected in the Breggia spawning site with the raw DoD and the 68% C.L. DoD are true redds, we measured the length of the tails and we estimated female lengths and the basal burial depths of eggs (Table 6).

Table 6: Estimated female length and basal burial depth from tail length for the Breggia Spawning site.

Date	Redd	Tail length (cm)	Estimated female length (cm)	Estimated egg burial depth (cm)
Nov. 19th	R1	166.9	48.9	16.7
Dec. 2nd	R2	68.3	23.2	6.3
Dec. 2nd	R3	72.2	24.3	6.9
Dec. 2nd	R4	74.2	24.9	7.3
Dec. 2nd	R5	47.4	17.1	2.1
Dec. 2nd	R6	76.9	25.63	7.7
Dec. 2nd	R7	92.3	29.8	9.8
Dec. 10th	R8	84.6	27.7	8.8
Dec. 10th	R9	149.7	44.7	15.5

Estimated female lengths vary from 17.1 cm to 48.9 cm with a mean size of 29.6 cm and a standard deviation of ±10.4 (Table 6). Curiously, four of six female lengths estimated for the Dec. 2nd are similar (σ_{length} = ±1.02), which might mean that it was only one instead of four female trout that produced R2,

R3, R4 and R6. The estimated female length for R5 seems to be too small (17.1 cm) for a sexually mature trout.

Estimated basal burial depths vary from the minimum of 2.1 cm to the maximum of 16.7 cm with a mean depth of 9 cm and a standard deviation of ±4.6 (Table 6). The estimated basal burial depths may be analysed to understand if later spawners eroded previous redds.

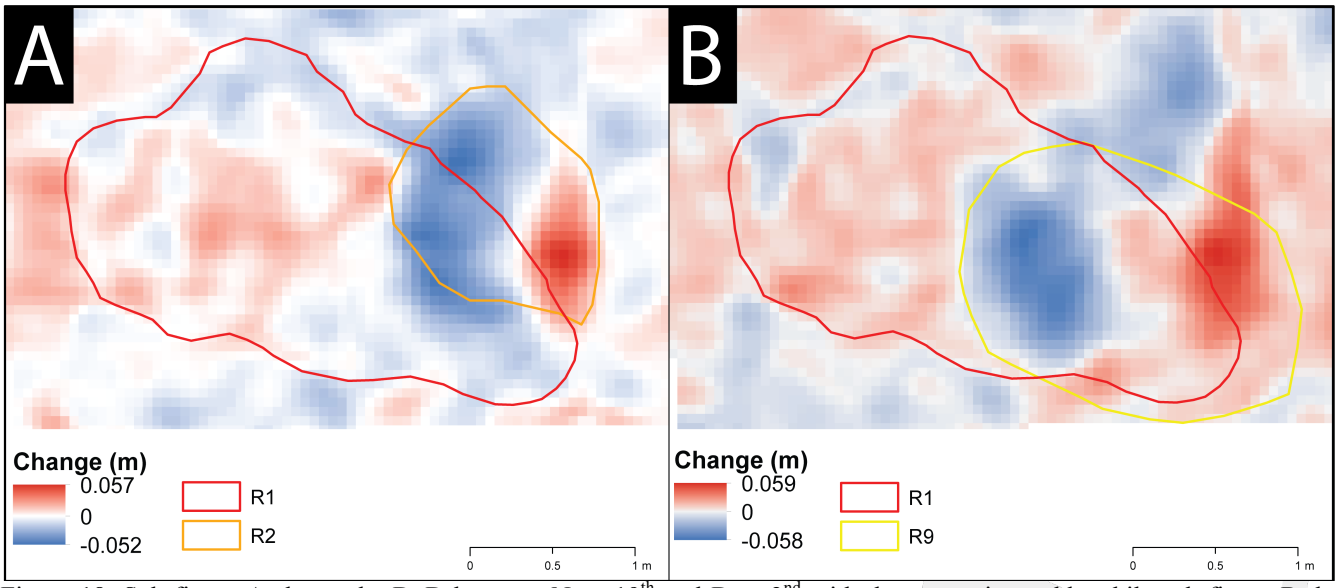

Figure 18: Sub-figure A shows the DoD between Nov. 19th and Dec. 2nd with the respective redds while sub-figure B the DoD between Nov. 19th and Dec. 10th with the respective redds.

From Figure 18 it appears that R2 was partially created on the tail sediments of R1, however the female erosion does not reach the egg basal burial depth of R1 because the maximum pit depth of R2 is 5.2 cm. In addition to this, the pit was created only on one side of R1 tail, reducing the probability of egg pocket destruction.

By contrast, the R9 pit was created totally on the R1 tail, which might mean that eggs located in R1 were moved away and consequently lost. However, as it was for R2, the maximum depth reached in the creation of R9 pit (5.8 cm) has not been so important to reach the basal burial depth of R1 (16.5 cm). Consequently, the sediments might have naturally protected eggs pockets located near the basal depth of R1 even if R9 pit was created where R1 eggs were laid. Clearly, one or more egg pockets might have been in upper layers and consequently they might have been destroyed by R9.

Even with doubt over R5 and a certain probability of some R9 egg pockets being destroyed, we finally consider a total of 9 redds in this 10 m reach of the Breggia site. We will discuss this in Section 6.

6. Discussion

The Discussion is divided into two parts. First, we discuss redd detection using a combination of UAVs and SfM photogrammetry. In particular we discuss the errors that resulted and we assess the framework proposed. Second, we discuss the information extracted from SfM-derived outputs to enhance knowledge of spawning sites.

6.1 Redd detection

6.1.1 UAV technology

UAV technology has the potential to allow coverage of areas of more than 10'000 m^2 (Carbonneau et al., 2012) at very low cost. The potential resolution of the images acquired is strength of UAVs (e.g. Lejot et al., 2007; Niethammer et al., 2012), and as implicit in [5], lower resolution imagery implies lower vertical prevision but allows higher flights so covering larger areas more rapidly (Westoby et al., 2012), and the operator has substantial opportunity to control data acquisition and quality (e.g. evaluate U_{crit}). This is why a critical element of the framework proposed here is the evaluation of the necessary theoretical vertical precision such that the UAV can be flown as high as possible so maximizing areal coverage.

Current developments of drone technology (e.g. GPS positioning) do not require manual-flight modes but allow for the use of pre-programmed flight paths, which can be designed to specifically to meet the requirements of subsequent post-processing (Carbonneau et al., 2012) and data quality that is sought. UAVs represent three weaker points. First, weather conditions may limit the use of UAVs, in particular strong winds and rain. Cold or hot temperatures can also limit the autonomy of batteries, reducing the performance of the drone. Second, battery autonomy is a key point in survey and planning, in fact the area covered by UAVs is strictly dependent on the autonomy of batteries and on the number of batteries carried with in the survey. Third, regulation restrictions refer to the legal principles regarding drone use and each country has normally its own. These rules may not only impact on whether or not UAV can be used but also how it has to be used. For instance, in Switzerland, line of sight has to be maintained during drone use, which restricts the spatial extent of any one flight path.

6.1.2 Error assessment

As illustrated in Section 5.1, at the first stage, our DEMs were all affected by a negative tilt effect, which means that all DEMs had systematic variations of Z compared with our reference. This creates DoD with dominant or totally erosion patterns (as showed by Figure 8). Our analysis showed that these DoD cannot be used for the detection of redds in DEMs of difference because the systematic error swamped the actual changes (Figure 8). This problem was reflected in the associated mean errors (Table 2) and error distributions (Figure 12A) between our reference DEM and the analysed DEMs. Tilt detection, without prior bathymetry correction, resulted in a substantial improvement in DEM quality (Table 3, Figures 9) but bathymetric correction was also needed to remove the mean error to negligible levels (Table 4, Figure 10) and to reproduce redds that were apparent in orthorectified images (Figures 11 and 13). It is worth noting that in this study, a tilt was found, rather than doming (e.g. James and Robson, 2014; Carbonneau and Dietrich, 2017), and this may reflect the survey design adopted here (multiple flying heights, inclusion of off-nadir imagery) which was designed to reflect existing

knowledge regarding optimal approaches to camera calibration (e.g. Robson et al., 1992; Wackrow and Chandler, 2011; James and Robson, 2014; Carbonneau and Dietrich, 2017).

Bathymetric correction was crucial to reconcile the effects of flow variability (potentially also erosion and deposition which influences water depths locally) upon streambed bathymetry. This demonstrates the importance of the bathymetric corrections identified by Westaway et al. (2000, 2001) and the solution developed by Dietrich (2017) for SfM photogrammetry.

The precision, as is expected, was not substantially impacted upon by either the tilt or the bathymetric correction, these reducing bias. The standard deviation of errors of ±10, ±13 and ±15 mm (Table 4) correspond to levels of detection of ±14, ±18 and ±22 mm with a 68% confidence level, and ±27, ±36 and ±42 mm at the 95% level. These latter values should be the same as the theoretically-predicted precision (U_{crit}) of ±24 mm (from [5]) given the survey design and UAV used, if all other influences on data error have been minimised. As shown only one LoD is really near U_{crit} (±27 mm); the other two LoD (±36 and ±42 mm) are higher (±12 and ±18 mm) compared with U_{crit}. These latter LoD reflect the small remaining negative deviations presented in Figure 12C. However results are encouraging, and suggest that [5] is a good means of identifying the survey design necessary for redd detection.

6.1.3 DoD assessment

Visual detection of redds (e.g. Crisp and Carling, 1989; Riedl and Peter, 2013), whether on foot or through a simple analysis of photos, has some weakness and a key finding from this research is the need to quantify redds and their dynamics in 3D using DoDs. Comparisons between Figures 13 and 15 show why interpretation of orthoimagery on its own is dangerous as it is not clear whether the redds are being destroyed, or whether they are being buried during general riverbed deposition. Figures 14 and 15 identify more redds than were visible in the orthoimagery (and would likely have been identified in a walkover survey).

We found some evidence to suggest that an LoD threshold at 68% was appropriate (e.g. Lane et al., 2003) as redd changes are spatially coherent and one possible development of what we report here would be to integrate the Wheaton et al. (2010) treatment of coherence in DEMs of difference so as to reduce the probability of false negatives (small magnitude but spatially coherent changes that fall within the 95% detection limits). Given the spatial coherence of redd related changes, a lower detection threshold seems to be appropriate.

6.2 Biological assessment

The Breggia spawning site does not only give us the possibility to demonstrate how new remote sensing technologies may help fish biology and water management but it also lends itself to a biological assessment. As introduced in Section 5.3, spawning began around Nov. 19th (first detected redd) and it ended around Dec. 10th (last detected redds), with a total season length of 21 days. The spawning time was relatively short compared with the literature, which proposes for Switzerland a long spawning season, from October to January (Riedl and Peter, 2013). As with previous research, spawning season depends on several biotic and abiotic factors such as genetic background (Quinn et al., 2000; Keller et al., 2011), river altitude (e.g. Riedl and Peter, 2013) and mean water temperatures (Heggberget et al., 1988; Webb and McLay, 1996; Klemetsen et al., 2003). In the absence of data about mean water temperatures at the Breggia spawning site, we assume that spawning began when the conditions for

reproduction were more suitable for brown trout. In this sense, and in addition to water temperatures, water velocities and water depths (see e.g. Armstrong et al., 2003) in the spawning site had to be ideal throughout these 21 days, or at least during the 9 spawning episodes.

The surface used to spawn by trout was small compared with the total wet surface investigated (see Figure 6). Here, the reason might be the limited availability of good spawning habitat (e.g. Armstrong et al., 2003), which confines spawning to such a small area. However, this also might mean a low productivity of the stretch. In this sense, Armstrong et al. (2003) argued that in case of a high density of spawners, some fish might be forced to spawn in poor habitat (e.g. outside the limits of the spawning area investigated), but the low density of spawning here suggests that this was not the case.

The data also suggested that redd superposition occurred throughout the season. Redd superposition is well documented in the scientific literature (e.g. Witzel and MacCrimmon, 1983; Sorensen et al., 1995) and it is typically explained by a limited spawning habitat availability (e.g. Ligon et al., 1995) or by spawning behaviour (Witzel and MacCrimmon, 1983; Essington et al., 1998). The two assumptions might both apply at our site. Following the behavioural point of view, Essington et al. (1998) argued that trout might choose a site previously used by another one just because it is more attractive, and not because habitat is limited. In this sense, as observed by Kondolf (2000), grain dislocations by earlier spawners might induce later spawners to use the same grounds just because grains are less compacted and they are easier to move. Redd superimposition has a biological relevance for the success of spawning. The construction of a new redd on top of a previous one normally means the dispersion and loss of the ancient eggs (e.g. Hayes, 1987). Our results suggest however that later redd pits do not reach the basal depth of the eggs pockets in the Breggia site, meaning that not all eggs have forcibly been washed-out. Egg pockets might be washed out if they were located in the upper sediments layers. This is also compounded by the possibility that flat, streambed-oriented stones in the sediment column under the redd sites have forced trout to lay their eggs at a lower depth (Crisp and Carling, 1989) compared with the predicted one

Another point to be assessed in the Breggia site is the presence of 4 redds with similar tail sizes (R2, R3, R4 and R6), which means similar female lengths. Here, it is possible that these 4 redds were constructed by the same female instead of four single females. However, a visual analysis of Dec. 2nd orthomosaic suggests that R5, R6 and R7 were constructed before R2, R3 and R4. This makes sense because the color gradients of R5, R6 and R7 are less important compared with the other three. Under this assumption, we suppose that there are high probabilities that a single female created R2, R3 and R4 in the same spawning period. Considering that a female usually creates only one redd per spawning season (Crisp, 2000), it is appropriate to believe that R3 and R4 are false redds without eggs. In fact, this can happen when the trout does not find satisfactory conditions after a first cut session and decides to abandon the site (Crisp, 2000). According to Gallagher et al. (2007), fresh and real redd pits clearly show the undisturbed sub-surface gravel-bed, which is normally composed of a dominant pebble matrix. R2 clearly shows this undisturbed gravel-bed while R3 and R4 show only a rough sediment matrix. This suggests that R3 and R4 were failed attempts to create a redd.

Some doubts also emerged regarding R5 because of its size, smaller than the others, and the consequent estimated female length. In fact, the estimated female length of 17.11 cm seems to be too small for a mature trout in a low altitude river like the Breggia. In the Platte River (Michigan, US), Taube (1976) recorded sexual maturity from 17.7 cm, however the majority of females were sexually mature from 20.2 to 22.7 cm. Even if the comparison with the Breggia is difficult, the data recorded by

Taube (1976) might validate our measurements for R5. There is also the possibility, nevertheless too complicated to demonstrate, that R5 is a false redd constructed by the R6 female.

From a biological point of view, doubts on the real extent of spawning in this site remain. These are compounded by the impossibility to know *a priori* (i.e. without look inside the redd, e.g. freeze-coring) if redds contain eggs or not.

7. Conclusions

Our results suggest that redds may be detected through the combination of UAVs and Structure-from-Motion photogrammetry. However, unlike before, we propose a different way to detect them in rivers, which uses morphological changes instead of color gradients. This is an important improvement in redd detection because morphological changes are less sensitive to the evolution of the streambed in normal hydraulic conditions. In this sense, we demonstrated that our new approach may be useful to detect not only the presence of redds but also their superposition, something that is particularly hard to identify visually. Crucial here is the derivation, correction and interpretation of DEMs of Difference, something that is increasingly straightforward given advances in our understanding of SfM photogrammetry.

This approach needs further investigation, because some disadvantages exist. Firstly, the switch from a visual approach to a morphological one still requires some dGPS data to aid the installation of ground control points. Such instruments are expensive and work should look at what happens when the GPS systems of UAVs, without GCPs, are used. This might involve co-registration using stable points visible on multiple images, or the kind of co-registration techniques that we used here to remove tilt. Second, image acquisition still takes time and is also dependent on the duration of battery autonomy during UAV flights. This means that survey design must be optimised, but thought also needs to be given to what is feasible during a redd detection study, as well as making sure that measurements are really focused on those reaches where spawning is feasible (e.g. excluding concrete sections) such that coverage at the watershed level can be increased. Such an approach also reduces data processing time, which can be considerable with large volumes of imagery. Finally, the proposed method does not work in fully or partially vegetation-covered rivers or with a high presence of obstacles (e.g. high voltage lines).

However and even with some disadvantages, the practical relevance of this method is also illustrated by the possibility of extracting information about spawning directly from DEMs of difference without redd disturbance or redd destruction.

8. References

Armstrong, J.D., Kemp, P.S., Kennedy, G.J.A., Ladle, M. (2003). Habitat requirements of Atlantic salmon and brown trout in rivers and streams. *Fisheries Research, 62*, 143-170. doi : 10.1016/S0165-7836(02)00160-1

Bergeron, N., Carbonneau, P.E. (2012). Geosalar: Innovative Remote Sensing Methods for Spatially Continuous Mapping of Fluvial Habitat at Riverscape Scale. In Carbonneau and Piégay (ed.), *Fluvial Remote Sensing for Science and Management* (pp. 193-213). Oxford: Wiley-Blackwell.

Besl, P. J., & McKay, N. D. (1992, April). Method for registration of 3-D shapes. In *Sensor Fusion IV: Control Paradigms and Data Structures* (Vol. 1611, pp. 586-607). International Society for Optics and Photonics. doi: 10.1117/12.57955

Bisson, P., Dunham, J., & Reeves, G. (2009). Freshwater ecosystems and resilience of Pacific salmon: habitat management based on natural variability. *Ecology and Society*, *14*(1). Available at https://www.ecologyandsociety.org/vol14/iss1/art45/main.html

Borsuk, M.E., Reichert, P., Peter, A., Schager, E., Burkhardt-Holm, P. (2006). Assessing the decline *Modelling*, *192*(1), 224-244. doi : 10.1016/j.ecolmodel.2005.07.006

Bradford, M.J., Irvine, J.R. (2000). Land use, fishing, climate change, and the decline of Thompson River, British Columbia, coho salmon. *Canadian Journal of Fisheries and Aquatic Sciences*, *57*(1), 13-16. doi : 10.1139/f99-283

Brasington, J., Rumsby, B. T., McVey, R. A. (2000). Monitoring and modelling morphological change in a braided gravel-bed river using high resolution GPS-based survey. *Earth Surface Processes and Landforms*, *25*(9), 973-990. doi: 10.1002/1096-9837(200008)25:9<973::AID-ESP111>3.0.CO;2-Y

Burner, C. J. (1951). *Characteristics of spawning nests of Columbia River salmon*. US Department of the Interior.

Butler, J.B., Lane, S.N., Chandler, J.H. (2001). Automated extraction of grain-size data from gravel surfaces using digital image processing. *Journal of Hydraulic Research*, *39*(5), 519-529. doi : 10.1080/00221686.2001.9628276

Carbonneau, P. E., Lane, S. N., & Bergeron, N. E. (2004). Catchment‐scale mapping of surface grain size in gravel bed rivers using airborne digital imagery. *Water resources research*, *40*(7). doi: 10.1029/2003WR002759

Carbonneau, P. E., Bergeron, N., Lane, S. N. (2005). Automated grain size measurements from airborne remote sensing for long profile measurements of fluvial grain sizes. *Water Resources Research*, *41*(11). doi: 10.1029/2005WR003994

Carbonneau, P.E., Piégay, H., Lejot, J., Dunford, R., Michel, K. (2012). Hyperspatial Imagery in Riverine Environments. In Carbonneau and Piégay (ed.), *Fluvial Remote Sensing for Science and Management* (pp. 163-191). Oxford: Wiley-Blackwell.Carbonneau, P. E.,

Carbonneau, P.E. and Dietrich, J.T. (2017). Cost‐effective non‐metric photogrammetry from consumer‐grade sUAS: implications for direct georeferencing of structure from motion photogrammetry. *Earth Surface Processes and Landforms*, *42*(3), 473-486. doi : 10.1002/esp.4012

Crisp, D.T. and Carling, P.A. (1989). Observation on siting, dimensions and structure of salmonid redds. *Journal of Fish Biology*, *34*(1), 119-134. doi : 10.1111/j.1095-8649.1989.tb02962.x

Crisp, D.T. (2000). *Trout and salmon: ecology, conservation and rehabilitation*. Hoboken : Wiley-Blackwell.

DeVries, P. (1997). Riverine salmonid egg burial depths: review of published data and implications for scour studies. *Canadian Journal of Fisheries and Aquatic Sciences*, *54*(8), 1685-1698. doi: 10.1139/f97-090

Dietrich, J.T. (2016). Riverscape mapping with helicopter-based Structure-from-Motion photogrammetry. *Geomorphology*, *252*, 144-157. doi : 10.1016/j.geomorph.2015.05.008

Dietrich, J.T. (2017). Bathymetric Structure-from-Motion: extracting shallow stream bathymetry from multi-view stereo photogrammetry. *Earth Surface Processes and Landforms*, *42*(2), 355-364. doi : 10.1002/esp.4060

Elliot, J.M. (1994). *Quantitative ecology and the brown trout*. New York : Oxford University Press Inc..

Essington, T. E., Sorensen, P. W., Paron, D. G. (1998). High rate of redd superimposition by brook trout (Salvelinus fontinalis) and brown trout (Salmo trutta) in a Minnesota stream cannot be explained by habitat availability alone. *Canadian Journal of Fisheries and Aquatic Sciences*, *55*(10), 2310-2316. doi: 10.1139/f98-109

Fisher, P.F. and Tate, N.J. (2006). Causes and consequences of error in digital elevation models. *Progress in Physical Geography*, *30*(4), 467-489. doi : 10.1191/0309133306pp492ra

Fonstad, M.A., Dietrich, J.T., Courville, B.C., Jensen, J.L., Carbonneau, P.E. (2013). Topographic structure from motion: a new development in photogrammetric measurement. *Earth Surface Processes and Landforms*, *38*(4), 421-430. doi : 10.1002/esp.3366

Fryer, J.G. (1983). A simple system for photogrammetric mapping in shallow water. *The Photogrammetric Record*, *11*(62), 203-208. doi : 10.1111/j.1477-9730.1983.tb00471.x

Fryer, J.G., Kniest, H.T. (1985). Errors In Depth Determination Caused By Waves In Through-Water Photogrammetry. *The Photogrammetric Record*, *11*(66), 745-753. doi : 10.1111/j.1477-9730.1985.tb01326.x

Fuller, I.C., Large, A.R., Charlton, M.E., Heritage, G.L., Milan, D.J. (2003). Reach-scale sediment transfers: An evaluation of two morphological budgeting approaches. *Earth Surface Processes and Landforms*, *28*(8), 889-903. doi : 0.1002/esp.1011

Gallagher S.P., Hahn, P.K.J., Johnson, D.H (2007). Redd counts. In D.H. Johnson, B.M. Shrier, J.S. O'Neal, J.A. Knutzen, X. Augerot, T.A. O'Neil and T.N. Pearsons (eds), *Salmonid Field Protocols Handbook* (pp. 197-234). Bethesda: American Fisheries Society.

Grost, R.T., Hubert, W.A., Wesche, T.A. (1991). Description of brown trout redds in a mountain stream. *Transactions of the American Fisheries Society*, *120*(5), 582-588. doi: 10.1577/1548-8659(1991)120<0582:DOBTRI>2.3.CO;2

Groves, P.A., Alcorn, B., Wiest, M. M., Maselko, J. M., Connor, W. P. (2016). Testing unmanned aircraft systems for salmon spawning surveys. *FACETS*, *1*(1), 187-204. doi: 10.1139/facets-2016-0019

Healey, M.C. (1991). Life history of chinook salmon (Oncorhynchus tshawytscha). In C. Groot and L. Margolis (eds.), *Pacific salmon life histories* (pp. 311-394). Vancouver: UBC Press

Harvey, A.H., Gallagher, J.S., Sengers, J. L. (1998). Revised formulation for the refractive index of water and steam as a function of wavelength, temperature and density. *Journal of Physical and Chemical Reference Data*, *27*(4), 761-774.
doi: 10.1063/1.556029

Hayes, J.W. (1987). Competition for spawning space between brown (Salmo trutta) and rainbow t rout (S. gairdneri) in a lake inlet tributary, New Zealand. *Canadian Journal of Fisheries and Aquatic Sciences*, *44*(1), 40-47.
doi: 10.1139/f87-005

Heggberget, T.G., Haukebø, T., Mork, J., Ståhl, G. (1988). Temporal and spatial segregation of spawning in sympatric populations of Atlantic salmon, Salmo salar L., and brown trout, Salmo trutta L. *Journal of Fish Biology*, *33*(3), 347-356.
doi: 10.1111/j.1095-8649.1988.tb05477.x

Hendry, K., Cragg-Hine, D., O'Grady, M., Sambrook, H., Stephen, A. (2003). Management of habitat for rehabilitation and enhancement of salmonid stocks. *Fisheries Research*, *62*(2), 171-192.
doi : 10.1016/S0165-7836(02)00161-3

James, M.R. and Robson, S. (2014). Mitigating systematic error in topographic models derived from UAV and ground-based image networks. *Earth Surface Processes and Landforms*, *39*(10), 1413-1420.
doi : 10.1002/esp.3609

James, M.R., Robson, S., d'Oleire-Oltmanns, S., Niethammer, U. (2017). Optimising UAV topographic surveys processed with structure-from-motion: Ground control quality, quantity and bundle adjustment. *Geomorphology*, *280*, 51-66.
doi: 10.1016/j.geomorph.2016.11.021

Jonsson, B. and Jonsson, N. (1993). Partial migration: niche shift versus sexual maturation in fishes. *Reviews in Fish Biology and Fisheries*, *3*(4), 348-365.
doi: 10.1111/j.1600-0633.2008.00322.x

Keller, I., Taverna, A., Seehausen, O. (2011). Evidence of neutral and adaptive genetic divergence between European trout populations sampled along altitudinal gradients. *Molecular ecology*, *20*(9), 1888-1904.
doi: 10.1111/j.1365-294X.2011.05067.x

Klemetsen, A., Amundsen, P.A., Dempson, J.B., Jonsson, B., Jonsson, N., O'connell, M.F., Mortensen, E. (2003). Atlantic salmon Salmo salar L., brown trout Salmo trutta L. and Arctic charr Salvelinus alpinus (L.): a review of aspects of their life histories. *Ecology of freshwater fish*, *12*(1), 1-59.
doi: 10.1034/j.1600-0633.2003.00010.x

Kondolf, G.M. (2000). Assessing salmonid spawning gravel quality. *Transactions of the American fisheries Society*, *129*(1), 262-281.
doi: 10.1577/1548-8659(2000)129<0262:ASSGQ>2.0.CO;2

Kondolf, G.M., Williams, J.G., Horner, T.C., Milan, D.A.V.I. D. (2008). Assessing physical quality of spawning habitat. In *American Fisheries Society Symposium* (Vol. 65, pp. 000-000).

Lane, S.N., Richards, K.S., & Chandler, J.H. (1994). Developments in monitoring and modelling small‐scale river bed topography. *Earth Surface Processes and Landforms*, *19*(4), 349-368.
doi: 10.1002/esp.3290190406

Lane, S.N., Westaway, M., Hicks, D.M. (2003). Estimation of erosion and deposition volumes in a large, gravel-bed, braided river using synoptic remote sensing. *Earth Surface Processes and Landforms*, *28*(3), 249-271.
doi : 10.1002/esp.483

Lane, S. N., Reid, S. C., Westaway, R. M., & Hicks, D. M. (2004). Remotely sensed topographic data for river channel research: the identification, explanation and management of error. In Kelly R.E.J., N.A. Drake and S.L. Barr, *Spatial Modelling of the Terrestrial Environment* (pp. 113-136). West Sussex: John Wiley & Sons, Ltd.

Lane, S. N., Widdison, P. E., Thomas, R. E., Ashworth, P. J., Best, J. L., Lunt, I. A., Sambrook Smith, G. H. & Simpson, C. J. 2010). Quantification of braided river channel change using archival digital image analysis. *Earth Surface Processes and Landforms*, *35*(8), 971-985. doi: 10.1002/esp.2015

Lejot, J., Delacourt, C., Piégay, H., Fournier, T., Trémélo, M.-L., Allemand, P. (2007). Very high spatial resolution imagery for channel bathymetry and topography from unmanned mapping controlled platform. *Earth Surface Processes and Landforms*, *32*(11), 1705-1725. doi : 10.1002/esp.1595

Ligon, F.K. (1995). Downstream Ecological Effects of Dams. *BioScience*, *45*(3), 183-192. doi: 10.2307/1312557

Lowe, D.G. (1999). Object recognition from local scale-invariant features. In *Computer vision, 1999. The proceedings of the seventh IEEE international conference on* (Vol. 2, pp. 1150-1157). Ieee. doi: 10.1109/ICCV.1999.790410

Marteau, B., Vericat, D., Gibbins, C., Batalla, R.J., Green, D.R. (2017). Application of Structure-from-Motion photogrammetry to river restoration. *Earth Surface Processes and Landforms*, *42*(3), 503-515. doi : 10.1002/esp.4086

Micheletti, N., Chandler, J.H., Lane, S.N. (2015a). Structure from motion (SFM) phogrammetry. In Cook, S.J., Clarke, L.E., Nield, J.M. (eds.), *Geomorphological Techniques* (Online Edition). British Society for Geomorphology: London.

Micheletti, N., Chandler, J.H., Lane, S.N. (2015b). Investigating the geomorphological potential of freely available and accessible structure-from-motion photogrammetry using a smartphone. *Earth Surface Processes and Landforms*, *40*(4), 473-486. doi : 10.1002/esp.3648

Milan, D.J., Heritage, G. L., Large, A. R., Fuller, I. C. (2011). Filtering spatial error from DEMs: Implications for morphological change estimation. *Geomorphology*, *125*(1), 160-171. doi: 10.1016/j.geomorph.2010.09.012

Nehlsen, W., Williams, J.E., Lichatowich, J.A. (1991). Pacific salmon at the crossroads: stocks at risk from California, Oregon, Idaho, and Washington. *Fisheries*, *16*(2), 4-21. doi : 10.1577/1548-8446(1991)016<0004:PSATCS>2.0.CO;2

Niethammer, U., James, M.R., Rothmund, S., Travelletti, J., Joswig, M. (2012). UAV-based remote sensing of the Super-Sauze landslide: Evaluation and results. *Engineering Geology*, *128*, 2-11. doi : 10.1016/j.enggeo.2011.03.012

Ottaway, E.M., Carling, P.A., Clarke, A., & Reader, N.A. (1981). Observations on the structure of brown trout, Salmo trutta Linnaeus, redds. *Journal of Fish Biology*, *19*(5), 593-607. doi: 10.1111/j.1095-8649.1981.tb03825.x

Pix4D (2017a). Pix4Dcapture. *Pix4D*. Available at https://pix4d.com/product/pix4dcapture (consulted the 21st may 2017).

Pix4D (2017b). Pix4Dmapper pro. *Pix4D*. Available at https://pix4d.com/product/pix4dmapper-pro/ (consulted the 21st may 2017).

Quinn, T.P., Unwin, M.J., & Kinnison, M.T. (2000). Evolution of temporal isolation in the wild: genetic divergence in timing of migration and breeding by introduced chinook salmon populations. *Evolution*, *54*(4), 1372-1385.
doi: 10.1554/0014-3820(2000)054[1372:EOTIIT]2.0.CO;2

Quinn, T.P. (2005). *The behaviour and ecology of Pacific Salmon and Trout*. Seattle: University of Washington Press.

Riedl, C. and Peter, A. (2013). Timing of brown trout spawning in Alpine rivers with special consideration of egg burial depth. *Ecology of Freshwater Fish*, *22*(3), 384-397.
doi : 10.1111/eff.12033

Rieman, B. E., & McIntyre, J. D. (1996). Spatial and temporal variability in bull trout redd counts. *North American Journal of Fisheries Management*, *16*(1), 132-141.
doi: 10.1577/1548-8675(1996)016<0132:SATVIB>2.3.CO;2

Robson, S. (1992). Film deformation in non-metric cameras under weak geometric conditions-an uncorrected disaster?. In *Intenrational Archives of Photogrammetry and Remote Sensing* (Vol. 29, No. B5, pp. 561-567). International Society for Photogrammetry and Remote Sensing.

Simenstad, C.A., Cordell, J.R. (2000). Ecological assessment criteria for restoring anadromous salmonid habitat in Pacific Northwest estuaries. *Ecological Engineering*, *15*(3), 283-302.
doi : 10.1016/S0925-8574(00)00082-3

Sorensen, P.W., Essington, T., Weigel, D.E., Cardwell, J.R. (1995). Reproductive interactions between sympatric brook and brown trout in a small Minnesota stream. *Canadian Journal of Fisheries and Aquatic Sciences*, *52*(9), 1958-1965.
doi: 10.1139/f95-787

Tamminga, A., Hugenholtz, C., Eaton, B., Lapointe, M. (2015). Hyperspatial Remote Sensing of Channel Reach Morphology and Hydraulic Fish Habitat Using an Unmanned Aerial Vehicle (UAV): A First Assessment in the Context of River Research and Management. *River Research and Applications*, *31*(3), 379-391.
doi : 10.1002/rra.2743

Taube, C.M. (1976). Sexual maturity and fecundity in brown trout of the Platte River, Michigan. *Transactions of the American Fisheries Society*, *105*(4), 529-533.
doi: 10.1577/1548-8659(1976)105<529:SMAFIB>2.0.CO;2

Wackrow, R., Chandler, J. H. (2011). Minimising systematic error surfaces in digital elevation models using oblique convergent imagery. *The Photogrammetric Record*, *26*(133), 16-31.
doi : 10.1111/j.1477-9730.2011.00623.x

Webb, J.H., and McLay, H.A. (1996). Variation in the time of spawning of Atlantic salmon (Salmo salar) and its relationship to temperature in the Aberdeenshire Dee, Scotland. *Canadian Journal of Fisheries and Aquatic Sciences*, *53*(12), 2739-2744.
doi: 10.1139/f96-240

Westaway, R.M., Lane, S.N., Hicks, D.M. (2000). The development of an automated correction procedure for digital photogrammetry for the study of wide, shallow, gravel-bed rivers. *Earth Surface Processes and Landforms*, *25*(2), 209-226.
doi : 10.1002/(SICI)1096-9837(200002)25:2<209::AID-ESP84>3.0.CO;2-Z

Westaway, R.M., Lane, S.N., Hicks, D.M. (2001). Remote sensing of clear-water, shallow, gravel-bed rivers using digital photogrammetry. *Photogrammetric Engineering and Remote Sensing*, *67*(11), 1271-1282.
Available at https://www.asprs.org/wp-content/uploads/pers/2001journal/november/2001_nov_1271-1281.pdf

Westoby, M.J., Brasington, J., Glasser, N.F., Hambrey, M.J., Reynolds, J.M. (2012). 'Structure-from-Motion' photogrammetry: A low-cost, effective tool for geoscience applications. *Geomorphology*, *179*, 300-314.
doi : http://dx.doi.org/10.1016/j.geomorph.2012.08.021

Wheaton, J.M., Brasington, J., Darby, S.E., Sear, D.A. (2010). Accounting for uncertainty in DEMs from repeat topographic surveys: improved sediment budgets. *Earth Surface Processes and Landforms*, *35*(2), 136-156.
doi : 10.1002/esp.1886

Williams, R.D. (2015). DEMs of Difference. In Cook, S.J., Clarke, L.E., Nield, J.M. (eds.), *Geomorphological Techniques* (Online Edition). British Society for Geomorphology: London

Witzel, L. D. and MacCrimmon, H. R. (1983). Embryo survival and alevin emergence of brook charr, Salvelinus fontinalis and brown trout, Salmo trutta, relative to redd gravel composition. *Canadian Journal of Zoology*, *61*(8), 1783-1792.
doi: 10.1139/z83-230

Woodget, A.S., Carbonneau, P.E., Visser, F., Maddock, I.P. (2015). Quantifying submerged fluvial topography using hyperspatial resolution UAS imagery and structure from motion photogrammetry. *Earth Surface Processes and Landforms*, *40*(1), 47-64.
doi : 10.1002/esp.3613

Zimmerli, S., Bernet, D., Burkhardt-Holm, P., Schmidt-Posthaus, H., Vonlanthen, P., Wahli, T., Segner, H. (2007). Assessment of fish health status in four Swiss rivers showing a decline of brown trout catches. *Aquatic Sciences-Research Across Boundaries*, *69*(1), 11-25.
doi : 10.1007/s00027-006-0844-3